Acta Geologica Sinica (English Edition), 2025, 99(1): 159–176

Investigating the Influence of Parent Rock and Sedimentation on the Diagenesis of Tuffaceous Clastic Rock: An Example from the Lower Cretaceous Junggar Basin, China

CHEN Sirui[1, 2], XIAN Benzhong[1, 2, *], JI Youliang[1, 2] and LI Jiaqi[3]

[1] *State Key Laboratory of Petroleum Resources and Prospecting, China University of Petroleum (Beijing), Beijing 102249, China*
[2] *College of Geosciences, China University of Petroleum (Beijing), Beijing 102249, China*
[3] *School of Energy Resources, China University of Geosciences, Beijing 100083, China*

Abstract: This study focuses on tuffaceous clastic rocks of the Lower Cretaceous Qingshuihe Formation in the southern margin of Junggar Basin. It aims to explore the influence of sedimentation and parent rock on this kind of reservoir development. The results show that the tuffaceous components formed by the denudation of ultramafic and mafic rocks can transform into chlorite coating or hematite, while those from intermediate rock denudation can be dissolved or transformed into illite. Sedimentary facies and lithofacies are essential in controlling the evolutionary result of tuffaceous components. Matrix-supported medium conglomerate and grain-supported medium-fine conglomerate that developed in the fan delta plain, with a closed original geochemical systems, have been in the oxidizing environment for a long time. The tuffaceous matrices mainly transforms into hematite or illite. These minerals occupy the primary pores and are difficult to dissolve by felsic fluids, which inhibits the development of high-quality reservoirs. The grain-supported sandy fine conglomerate developed in the fan delta front was in the underwater reductive environment with an open original geochemical system. The tuffaceous matrices not only can transform into chlorite coating to strengthen the particle's compaction resistance, but also can be fully dissolved, which promotes the formation of high-quality reservoirs.

Key words: sedimentation, parent rock, tuffaceous clastic rock, Lower Cretaceous, southern margin of Junggar Basin

Citation: Chen et al., 2025. Investigating the Influence of Parent Rock and Sedimentation on the Diagenesis of Tuffaceous Clastic Rock: An Example from the Lower Cretaceous Junggar Basin, China. Acta Geologica Sinica (English Edition), 99 (1): 159–176. DOI: 10.1111/1755-6724.15273

1 Introduction

In recent years, industrial oil-gas resources have been explored in tuffaceous clastic rocks globally, which have attracted wide attention (Summa and Verosub, 1992; Liu et al., 2019; Cicerali et al., 2020; Luo et al., 2020; Fang et al., 2021; Rutman et al., 2021; Martínez-Paco et al., 2022; Yang et al., 2023). Tuffaceous components, formed by volcanic eruptions, can be transported to lacustrine basins through fluvial-deltaic systems and subsequently deposited (Cui et al., 2022). However, due to the poor chemical stability (Summa and Verosub, 1992; Zhu et al., 2016; Cui et al., 2022), tuffaceous components are likely to occur a series of complicated diagenesis after deposition and maintain a long time (Hay and Guldman, 1987; Antibus et al., 2014; Benavente et al., 2015; Calvin et al., 2015; Zhu et al., 2019; Cui et al., 2022) As a result, the diagenetic process of tuffaceous clastic rock reservoirs is more intricate compared to clastic rock reservoirs without tuffaceous components. Studies have shown that tuffaceous components can improve reservoir quality through dissolution or transform into quartz cement, illite and mixed-layer illite/smectite through alteration and occupy the reservoir space (Bien et al., 1958; De La Fuente et al., 2000; Kiipli et al., 2007; Hong et al., 2019; Wei et al., 2020; Yang et al., 2023). Simultaneously, the diagenetic evolutionary results of tuffaceous components in different diagenetic environments also significantly differ. For instance, tuffaceous components are easily dissolved in felsic diagenetic environments but undergo alteration in alkaline environments (Hong et al., 2017; Zhu et al., 2019; Jin Z H et al., 2023). Therefore, to accurately predict and appraise the distribution of high-quality tuffaceous clastic rock reservoirs, it is necessary to conduct detailed studies on the controlling factors that can affect the diagenetic evolutionary results of tuffaceous components and determine which geological conditions cause constructive or destructive diagenetic evolution. Such research holds significant importance for the worldwide exploration of tuffaceous clastic rock reservoirs.

The Lower Cretaceous Qingshuihe Formation tuffaceous clastic reservoirs of well GT1 in the southern margin of the Junggar Basin have achieved a significant

* Corresponding author. E-mail: xianbzh@cup.edu.cn

breakthrough in oil-gas exploration, producing 12.13 × 10^4 m^3/d of oil and 320 × 10^3 m^3/d of natural gas (Du et al., 2019; Zhang et al., 2020). However, several appraisal wells around this well produced less oil and gas in the same formation, indicating that the tuffaceous clastic reservoirs have substantial heterogeneity (Gao et al., 2023; Jin J et al., 2023). Previous studies have primarily focused on explaining the heterogeneity of tuffaceous clastic rock reservoirs by analyzing their microscopic characteristics (Luo et al., 2020; Zhu et al., 2020). They believe that the complex and variable diagenetic environment is a main factor in determining the evolutionary outcome of tuffaceous components (Wei et al., 2016, 2018, 2019; Zhu et al., 2016; Jin Z H et al., 2023; Yang et al., 2023). However, few studies have focused on the impact of primary parent rock properties and initial sedimentary environments on the evolutionary result of tuffaceous components. Due to the variety of parent rock types in the provenance area, their geochemical properties also differ. Therefore, tuffaceous components formed by denudation from different parent rocks will release different ions during diagenetic evolution, potentially leading to diverse evolutionary outcomes for these components (Zhu et al., 2016; Wei et al., 2018). Additionally, differences in initial porosity, permeability, pore structure, and geochemical systems among various sedimentary environments may also significantly influence the evolutionary results of tuffaceous components. Therefore, it is obviously insufficient to explain the diagenetic heterogeneity of tuffaceous clastic rock reservoirs only from the perspective of the diagenetic environment's change; this approach cannot provide reliable theoretical guidance for predicting and evaluating high-quality reservoirs.

Therefore, this paper selected the tuffaceous clastic reservoirs of the Lower Cretaceous Qingshuihe Formation in the southern margin of the Junggar Basin as the research objects. The sedimentary environments of these reservoirs were determined by analysing the lithofacies and their assemblages. Simultaneously, the diagenetic characteristics, reservoir space, and physical properties were studied using mineralogy and petrology testing methods, such as thin-section observation, scanning electron microscopy (SEM), X-ray fluorescence spectroscopy (XRF), energy-dispersive spectroscopy (EDS), and electron probing analysis. The purposes aim to (1) determine the influence of sedimentation and geochemical properties of parent rocks on the diagenesis and reservoir quality of tuffaceous clastic rocks and (2) explore the development law of tuffaceous clastic reservoirs and provide more ideas for the efficient exploration and development of similar oil-gas reservoirs worldwide.

2 Geological Setting

The Junggar Basin is in the northern Xinjiang Uygur Autonomous Region of China, with an area of approximately 13 × 10^4 km^2 (Fig. 1a) (Xiao et al., 2020; Zhou et al., 2022). It is a sizeable, superimposed foreland basin with abundant oil-gas resources in northwest China (Xiao et al., 2020; Cheng et al., 2023; Lai et al., 2023). The southern margin of the Junggar Basin is adjacent to the Yilinheibiergen Mountains (Fig. 1b), which is 3 × 10^4 km^2 and stretches 500 km east–west (Zhou et al., 2022). From north to south, it is approximately 40–90 km wide (Zhou et al., 2022). The Sikeshu sag locates to the west of the southern margin of the Junggar Basin (Fig. 1b), bounded by the Yilinheibiergen Mountains in the south and the Zhayler Mountains in the west (Fig. 1b), showing an NWW–SEE strike of approximately 6.3 × 10^3 km^2 (Gao et al., 2013).

The study area is in the Gaoquan area of the southern Sikeshu sag (Fig. 1c). The study formation is the Lower Cretaceous Qingshuihe Formation (Fig. 1d). The burial depth of the clastic rock reservoirs of the Qingshuihe Formation is 5900–6100 m, and the diagenetic stage is in the eodiagenetic B stage to meso-diagenetic A stage (Gao et al., 2023; Jin J et al., 2023). From a sedimentation perspective, the clastic rock reservoirs of the Qingshuihe Formation comprise conglomerate and sandy conglomerate developed in multi-phase distributary channels of the fan delta plain or fan delta front (Gao et al., 2023). During the period from the Upper Jurassic to the Lower Cretaceous, large-scale volcanic activities occurred in the southern margin of the Junggar Basin, and the surrounding orogenic belt was rapidly uplifted and denudated (Li et al., 2012; Zhou et al., 2019; Cao Y Y et al., 2020), which leads to the development of tuffaceous components in the Qingshuihe Formation.

3 Data and Methods

This study's data included cores of approximately 60 m from five drilling wells for lithofacies classification, 80 thin sections for mineral composition statistics, morphology observation by SEM and geochemical composition analysis through EDS of 21 core samples, electron probing analysis of eight core samples and XRF analysis of 10 core samples. Furthermore, the porosity and permeability data applied to reservoir property analysis were collected from the Research Institute of Petroleum Exploration and Development of the Xinjiang Oilfield Company, PetroChina.

First, the classification of lithofacies and corresponding characteristic descriptions were performed based on approximately 60 m cores from wells G101, G103, GQ5, GQ6, and GHW001 in the study area. Then, 80 thin sections were made to analyse the characteristics of petrology, mineralogy and reservoir space. Each thin section was saturated with blue epoxy to identify different pores. All thin sections were partly stained with Alizarin Red S and K-ferricyanide for carbonate mineral identification (Dickson, 1965). We counted 300 points on each thin section to obtain the sandstone composition data in sandy conglomerate. For the tuffaceous matrix and cement contents, 16 micrographs of each blue epoxy resin-impregnated thin section were taken using the OLYMPUS-BX51 digital transmission microscope. Then, the tuffaceous matrix and cement in each micrograph were identified under the microscope. Finally, the tuffaceous matrix and cement percentages were calculated using the average values in the 16 micrographs from each thin

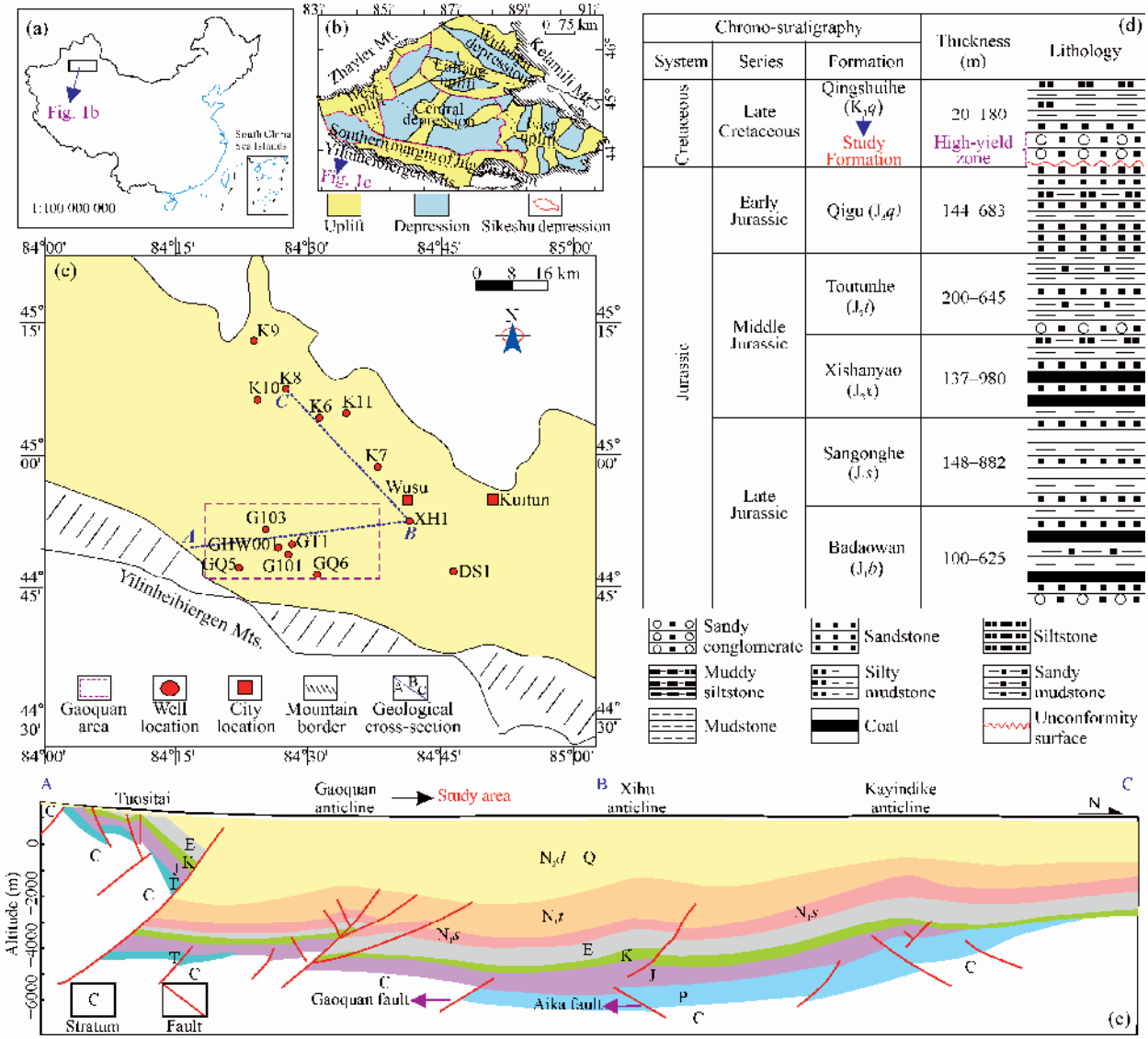

Fig. 1. Geological overview of the study area.

(a) Location map of the Junggar Basin in northwestern China (China basemap after China National Bureau of Surveying and Mapping Geographical Information); (b) sub-tectonic units of the Junggar Basin and location of the Southern margin of Junggar Basin; (c) well locations and fault distributions of the Sikeshu Sag; (d) generalized Lower Cretaceous Qingshuihe Formation stratigraphy in the Gaoquan area, Sikeshu Sag (C: Carboniferous; P: Permian; T: Triassic; J: Jurassic; E: Paleogene; N: Neogene; N_1s: Shawan Formation; N_1t: Taxihe Formation; N_2d: Donggou Formation; Q: Quaternary) (modified from Hu et al., 2017).

section (Xi et al., 2019; Yang et al., 2020).

Based on the thin-section analysis, 21 core samples were observed by a ZEISS Crossbeam 540-scanning electron microscope equipped with an energy-dispersive spectrometer (EDS). The Quanta FEG 450 energy-dispersive spectrometer was used to make semi-quantitative estimations of the geochemical elements of tuffaceous fragments, tuffaceous matrix and other diagenetic minerals. According to the point-count data, cement identification and the formulas proposed by Lundegard (1992) and Ehrenberg (1995), the compaction porosity loss (COPL) and the cementation porosity loss (CEPL) were estimated quantitatively to characterise the compaction and cementation intensity, respectively,

$$\mathrm{COPL} = \mathrm{OP} - [(100 - \mathrm{OP}) \times \mathrm{IGV}]/(100 - \mathrm{IGV}) \quad (1)$$

$$\mathrm{CEPL} = (\mathrm{OP} - \mathrm{COPL}) \times (\mathrm{CEM}/\mathrm{IGV}) \quad (2)$$

where, OP is the original porosity of the clastic rock reservoirs, assumed to be 40% for the calculations (Houseknecht, 1987), which is the volume percentage of intergranular cement. IGV is the intergranular volume to rock volume percentage, calculated using the sum of the tuffaceous matrix volume, intergranular porosity and the volume of intergranular cement (Wang et al., 2019).

Based on thin-section and SEM analysis, the element geochemistry of tuffaceous components without alteration in 33 samples was used for the quantitative estimation using a JXA-8100 electron probe micro-analyser (EPMA) with a spatial resolution up to 7 nm (measuring accuracy of ±1.0 wt% for major elements, and ±3.0 wt% for trace elements). Based on the dimensions of authigenic minerals, the beam size for EPMA was 3–5 μm. All

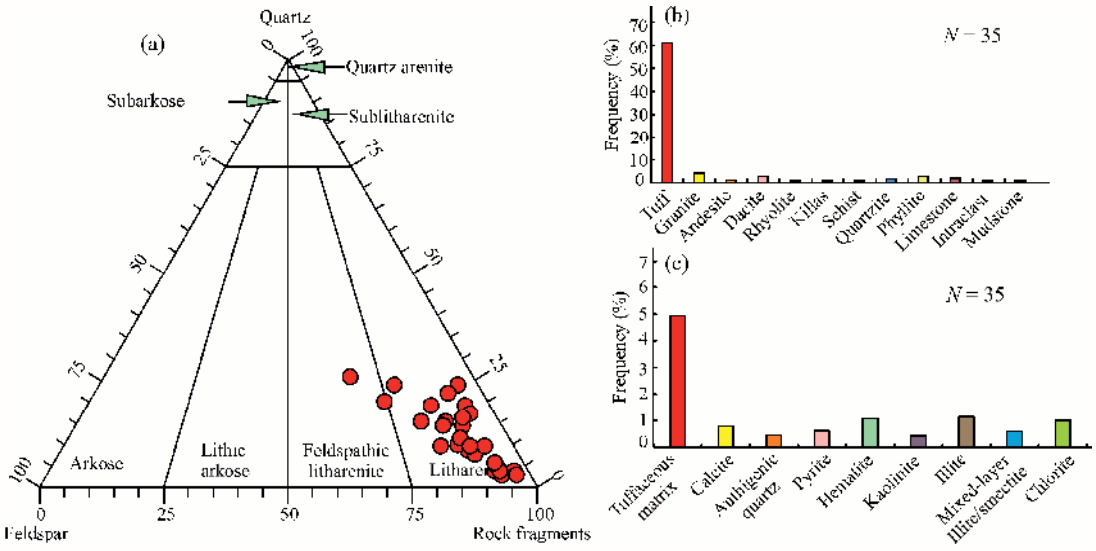

Fig. 2. Rock composition of clastic rock reservoirs of Qingshuihe Formation in the Gaoquan area, Sikeshu sag.
(a) Histogram showing the abundances of the various types of rock fragments; (b) histogram showing the abundances of the various types of interstitial materials.

elements were calibrated based on natural and synthetic standards using the following materials (Xi et al., 2021): SrO-celestite, Na_2O-albite, MgO-diopside, SiO_2-diopside, K_2O-sanidine, CaO-diopside, TiO_2-benitoite, FeO-hematite, MnO-bustamite and Cr_2O_3-chromium oxide.

Furthermore, the Bruker M4 Tornado high-performance X-ray fluorescence spectrometer was used to investigate the element distribution of the clastic particles of 10 thin sections without cover slides to analyse their parent rock geochemical properties. Each section was placed in a chamber using an X-ray diffractometer with Rh radiation. A silicon drift detector with a chip area of 30 mm^2, energy resolution (Mn Ka) smaller than 145 eV @ 300 Kcps and beam size of 40 μm was used to measure the element content and distribution from Na^{11} to U^{92} by scanning the thin section without cover slides.

4 Results

4.1 Rock component and types of parent rock

4.1.1 Rock component

According to the statistical results, the tuffaceous components occupy an exceptionally high proportion in the clastic rock reservoirs of the Qingshuihe Formation (Fig. 2a). The average content of tuffaceous fragments was 60.00%, the highest among all fragments (Fig. 2b). Observations of thin sections show that none of these tuffaceous fragments are more than 2 cm in diameter (Fig. 6). Similarly, the average range of tuffaceous matrix was 4.95%, accounting for the highest proportion among all interstitial materials (Fig. 2c).

4.1.2 Types of parent rock

The analysis results of X-ray fluorescence spectra show that the main element distribution of tuffaceous fragments in the Qingshuihe Formation displays a strong heterogeneity at the thin-section scale. According to 2D element scanning images, Si, Al and K of the tuffaceous fragments in well G103 are high, whereas Fe and Mg are low (Fig. 3). However, the tuffaceous fragments in well G101 were poor in Si, Al and K but rich in Fe and Mg (Fig. 3). Furthermore, all the above elements are enriched in the tuffaceous fragments in well GHW001 (Fig. 3).

Fragments are products of weathering and denudating of parent rocks in the provenance area (Dickinson et al., 1983; Bajestani et al., 2018). The XRF element scanning results indicate that the tuffaceous fragments in the clastic rock reservoirs of the Qingshuihe Formation come from different parent rocks. We use the total alkali–silica (TAS) plots proposed by Irvine and Baragar (1971) to identify the parent rock types of tuffaceous fragments of the Qingshuihe Formation. The element data points of the tuffaceous fragments from well G101 are concentrated in zones A and B, indicating that the parent rock type is primarily ultramafic (Fig. 4). The distribution zone of element data points in well G103 focuses on zone J, indicating that trachyte andesite (intermediate rock) dominates the parent rock (Fig. 4). The data points in well GHW001 primarily distribute in zones H and I, and the parent rock types are mixed with intermediate and mafic rocks (Fig. 4). Based on the above analysis, the parent rocks of tuffaceous fragments in the clastic rock reservoirs of the Qingshuihe Formation include ultramafic, mafic and intermediate rocks.

As another denudation product of the parent rocks in the provenance area, the matrix also inherits the geochemical characteristics of the parent rocks (Anda, 2012; Hong et al., 2019). By analysing the distribution characteristics of geochemical elements in the ternary diagram, the tuffaceous matrix of the Qingshuihe Formation can divide into three types. The Group-I tuffaceous matrix has low FeO and MgO but high SiO_2 and K_2O, indicating that their corresponding parent rocks belong to the category of intermediate rocks (Fig. 5). However, the Group-III tuffaceous matrix has high FeO and MgO but low SiO_2 and K_2O (Fig. 5), reflecting that it is the denudation

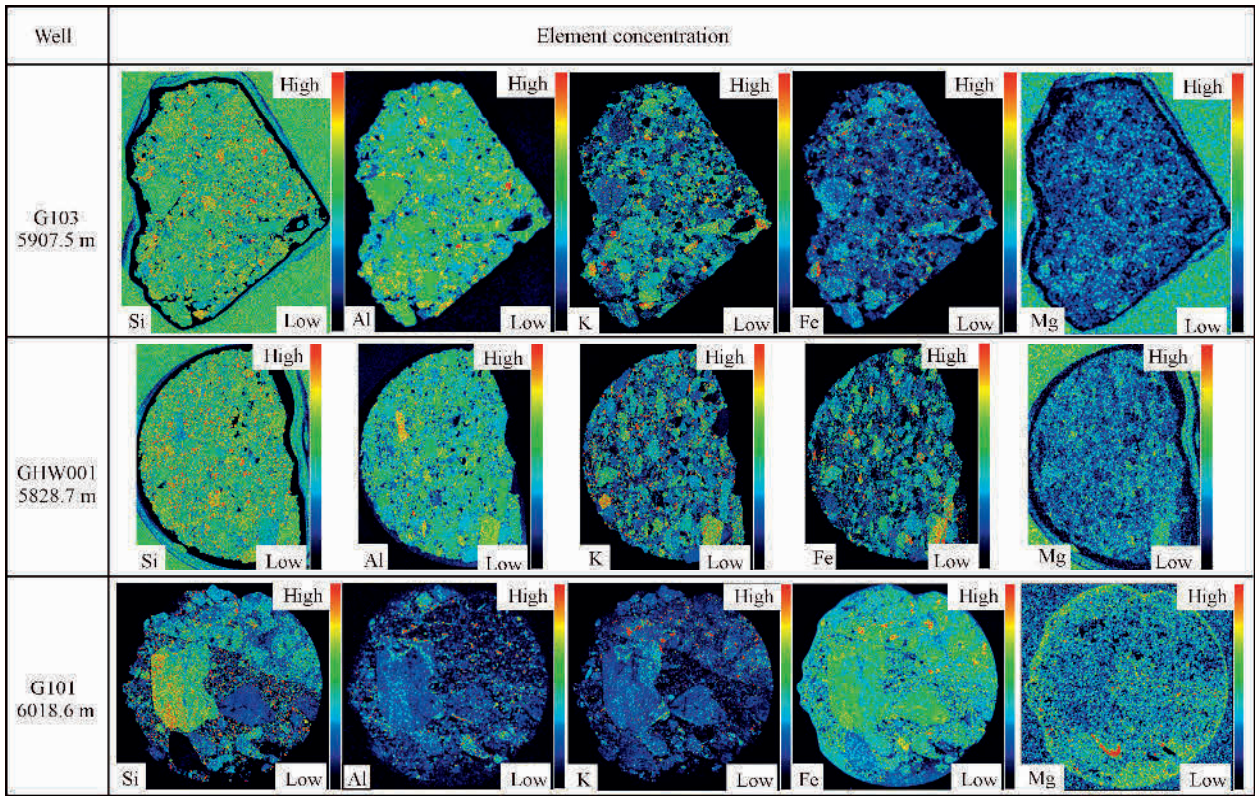

Fig. 3. The X-ray fluorescence (XRF) elemental maps showing the distribution and content of Si, Al, K, Fe and Mg in the tuffaceous fragments of Qingshuihe Formation in the Gaoquan area, Sikeshu Sag (the location of the cored well is shown in Fig. 1c).

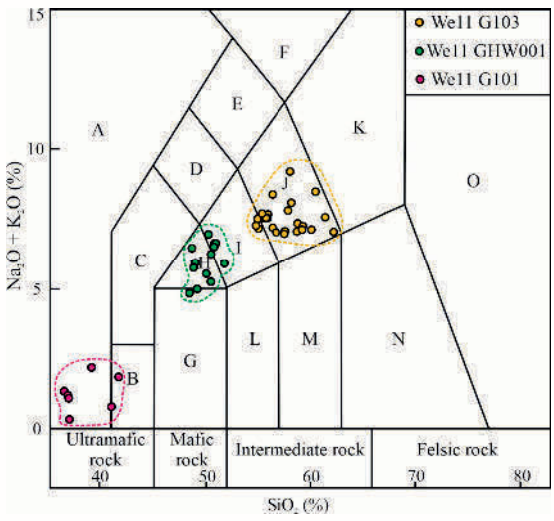

Fig. 4. Plot of TAS of tuffaceous fragments in the clastic rock reservoirs of Qingshuihe Fm., which is applied to identify the parent rock properties of tuffaceous fragments. A: foidite; B: picro-basalit; C: tephri-basanite; D: photo-tephrite; E: tephri-phonolite; F: phonolite; G: basaltic; H: trachy-basalt; I: basaltic trachyandesite; J: trachy andesite; K: trachyte trachydacite; L: basaltic andesite; M: andesite; N: dacite; O: rhyolite; the location of the cored well is shown in Fig. 1c.

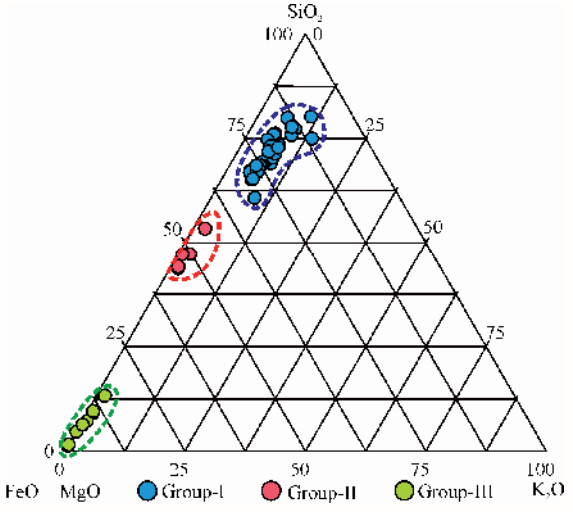

Fig. 5. Ternary diagrams showing elemental geochemistry (%) characteristics of tuffaceous matrix in the Qingshuihe Formation tuffaceous clastic reservoirs of Gaoquan area, Sikeshu sag.

product of ultramafic parent rocks (Fig. 5). The FeO, MgO, K_2O and SiO_2 contents in the Group-II tuffaceous matrix are between Group-I and Group-III. However, since the FeO content is much higher than that of Group-I (Fig. 5), Group-II tuffaceous matrix can be determined as the denudation product of bare rocks.

4.2 Lithofacies and depositional units

4.2.1 Lithofacies types and characteristics

Studies have shown that lithofacies can affect reservoir quality (Abdel-Fattah et al., 2022; Fu et al., 2022; Ye et al., 2022). Based on the analysis of core colour, grain size,

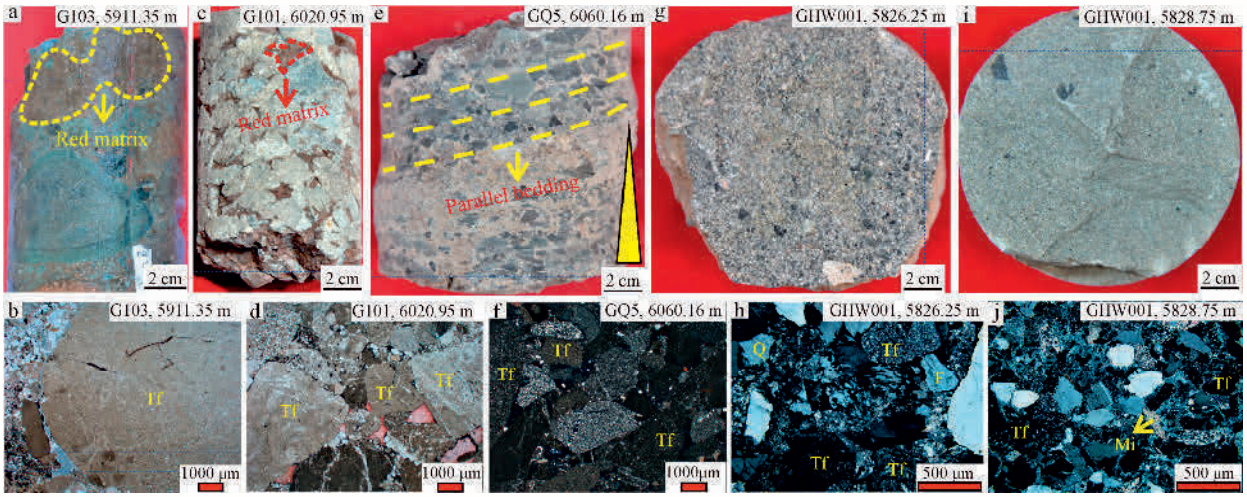

Fig. 6. Representative core photographs and photomicrographs of various lithofacies of Qingshuihe Formation in the Gaoquan area, Sikeshu sag.

(a, b) Matrix-supported medium conglomerate, the sample comes from sample-1 at well G103; (c, d) grain-supported medium-fine conglomerate, the sample comes from sample-2 at well G101; (e, f) grain-supported sandy fine conglomerate, the sample comes from sample-3 at well GQ5; (g, h) grain-supported coarse sandstone, the sample comes from sample-4 at well GHW001; (i, j) grain-supported fine sandstone, the sample comes from sample-5 at well GHW001. The sample point can be found in the Fig. 7. Tf: tuffaceous fragments; Q: quartz; F: feldspar; Mi: mica. The location of the cored well is shown in Fig. 1c.

texture and sedimentary structure, five lithofacies in the study area were recognised (Supp. Table 1), including matrix-supported medium conglomerate (Mmc), grain-supported medium–fine conglomerate (Gmfc), grain-supported sandy fine conglomerate (Gsfc), grain-supported coarse sandstone (Sc) and grain-supported fine sandstone (Sf).

The Mmc comprises grey or grey-green medium-grained gravel with matrix support and poor sorting characteristics. The shape (type: tuff) is semi-circular to circular gravel, and their grain size ranges from 4 mm to 8 mm (Fig. 6a and b). A large amount of matrix filled the intergranular pores, which are brick red (Fig. 6a). The contact relationship between gravel is primarily non-contact and point-contact, and some gravels seem to float in the matrix (Fig. 6a).

Gmfc comprises medium and fine gravel with grain support, and the gravels are mainly tuff (Fig. 6c, d). The contact relationship between gravels is point and line contact (Fig. 6c), and the content of brick red matrix between gravels is slightly lower than that of matrix-supported medium conglomerate (Fig. 6c).

Gsfc comprises fine grey-green gravel with 2–3 mm grain size and coarse sandstone (Fig. 6e, f). The morphology of fine gravels is sub-angular to sub-circular, with good sorting and low content of intergranular matrix (Fig. 6e). Also, the parallel bedding can be observed locally in the cores (Fig. 6e).

Sc comprises grey and dark grey coarse sandstone with grain support, good sorting and low matrix content (Fig. 6g). The grain size is concentrated in the range of 0.5–1 mm, and a small part of sandstones has a grain size of 1–2 mm (Fig. 6g, h).

Sf comprises fine grey-green sandstone with a grain size of 0.1–0.25 mm (Fig. 6i). The Sf has good sorting, and the intergranular pores contain mica minerals (Fig. 6j).

4.2.2 Lithofacies association (LA)

Based on the lithofacies types and vertical stacking patterns, the above-described five lithofacies of the Qingshuihe Formation can be grouped into seven LAs. LA1 comprises Gsfc with the characteristic of vertical stacking (Fig. 7). The thickness is 0.5–1.5 m, with an average value of 0.89 m. LA2 contains Gmfc, Gsfc and Sc (Figs. 6c, e, g, 7). The thickness range of LA2 is 1.0–2.8 m, and the thickness of Gmfc accounts for 87%–91%, indicating that this lithofacies is the primary part of LA2. Brick red Gmfc, greyish-green Gsfc and Sc indicate that LA2 has undergone alternating changes between oxidising and reductive environments (Fig. 6c, e, g). The distribution area of brick red is larger than that of grey-green (Fig. 7), indicating that LA2 has been in the onshore oxidising environment for a longer time.

LA3 comprises Gmfc and Gsfc with normally graded characteristics (Figs. 6c, e, 7). The Gmfc is the primary part of LA3, accounting for 90%. The distribution area of brick red in LA3 is much larger than that of grey-green (Fig. 7), indicating that LA3 has been in the oxidising environment for a long time.

LA4 comprises Gsfc, Sc and Sf successively from the bottom to the top, with normally graded characteristics (Figs. 6e, g, i, 7). The Gsfc is the primary part of LA4, accounting for 80%, whereas Sc and Sf only account for 10% each.

LA5 contains Gsfc and Sc with normally graded characteristics (Fig. 7), where Gsfc is the main part of LA5.

LA6 consists of Gsfc and Sc (Figs. 6e, i, 7), with typically graded characteristics, where Gsfc is the primary part of LA6.

LA7 entirely comprises Mmc (Figs. 6a, 7) with a thickness of 1.0–1.5 m, and the large distribution area of brick red indicates that LA7 is in an oxidising environment (Fig. 7).

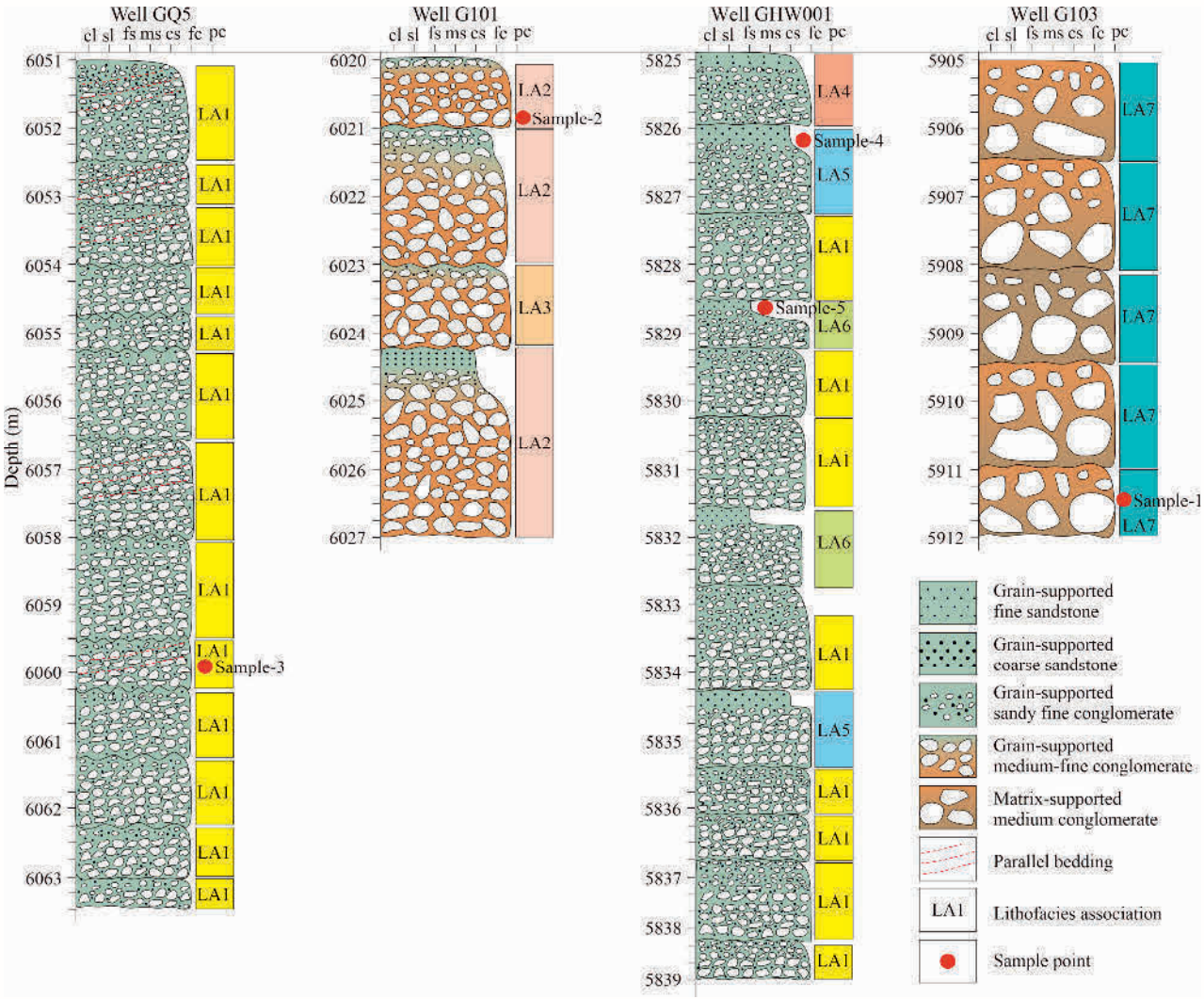

Fig. 7. Section of lithofacies, lithofacies association and depositional unit of Qingshuihe Formation in the Gaoquan area, Sikeshu sag.

Based on the above analysis, the Qingshuihe Formation primarily develops three lithofacies assemblages, including LA1, LA2 and LA7 (Fig. 8). Therefore, the Mmc, Gmfc and Gsfc can represent the primary lithofacies types in the Qingshuihe Formation clastic rock reservoirs (Fig. 8).

4.3 Diagenesis of tuffaceous clastic rock

The diagenetic types of the Qingshuihe Formation clastic rock reservoirs in the study area include mechanical compaction, alteration and dissolution.

4.3.1 Mechanical compaction

Mechanical compaction is essential in decreasing intergranular volume (Chester et al., 2004; Ajdukiewicz et al., 2010; Taylor et al., 2010). The compaction of the Qingshuihe Formation is strong, but the compaction intensity of different lithofacies differs significantly. The contact relationship between detrital particles in the Mmc and Gmfc includes line and concavo-convex contact, indicating strong compaction indirectly (Fig. 9a, b). However, the contact relationship of detrital particles in Gsfc primarily includes point and point-line contact, indicating weak compaction (Fig. 9c).

4.3.2 Component alteration

This study defines tuffaceous fragments and matrix as tuffaceous components. After the tuffaceous components are deposited in the basin, their alteration occurs easily (Zhu et al., 2016; Cui et al., 2022). The alteration products of tuffaceous components are primarily affected by their geochemical properties, formation temperature, formation pressure and diagenetic environment (Worley et al., 1996; Castro et al., 2008; Rowe et al., 2012; Hellevang et al., 2013; Zheng et al., 2018). The clastic rocks of the Qingshuihe Formation in the study area have similar burial–thermal history and burial depth (indicating similar temperature-pressure fields) (Gao et al., 2023), and their diagenetic stages are in the eodiagenetic B stage to meso-diagenetic A stage (meaning similar diagenetic environments) (Gao et al., 2023; Jin J et al., 2023). Therefore, the geochemical properties of tuffaceous components are essential for the types of alteration products.

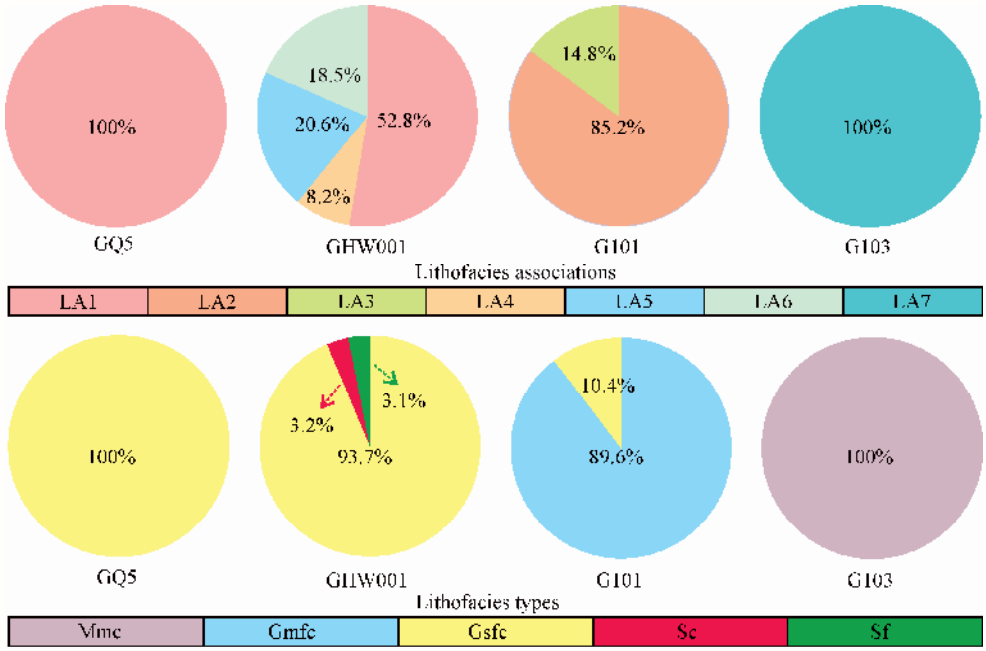

Fig. 8. The proportion of lithofacies and lithofacies association in the Qingshuihe Formation in the Gaoquan area, Sikeshu sag.

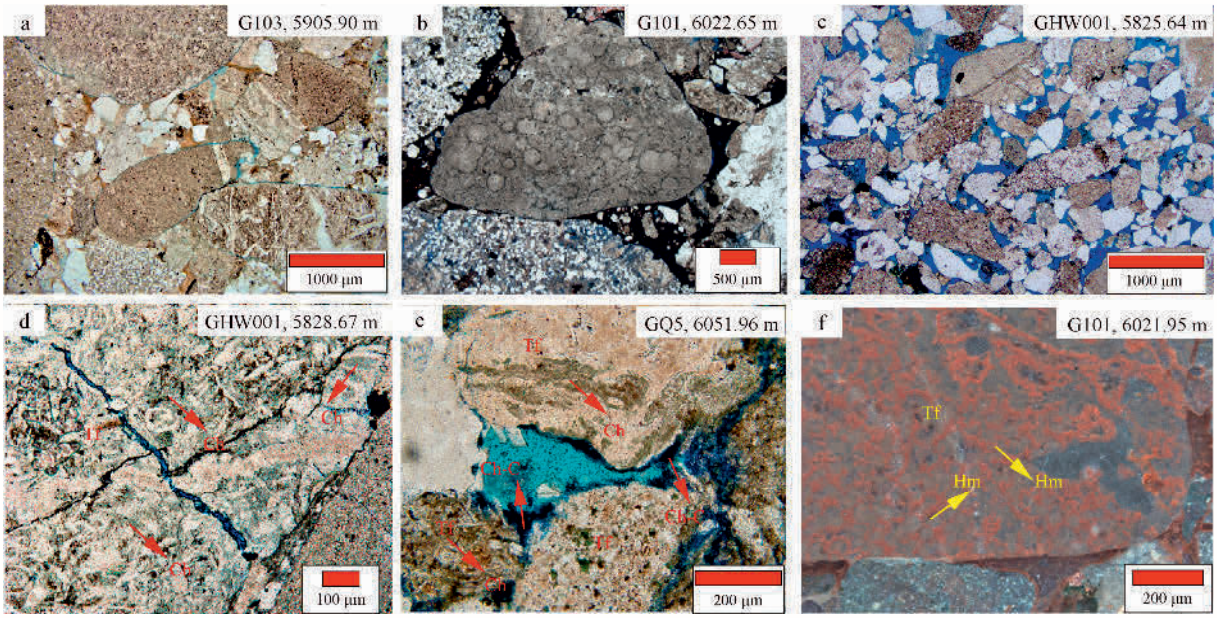

Fig. 9. Mechanical compaction characteristics of clastic rock reservoirs and alteration characteristics of tuff debris of Qingshuihe Formation in the Gaoquan area, Sikeshu sag.

(a) Matrix-supported medium conglomerate, (PPL), showing the relationship of grain-contacts is mostly linear to concavo-convex; (b) grain-supported medium-fine conglomerate(PPL), showing the relationship of grain-contacts is mostly linear; (c) grain-supported sandy fine conglomerate (PPL), showing the degree of mechanical compaction is relative weak; (d) grain-supported sandy fine conglomerate (PPL), showing altered tuffaceous fragments and precipitated chlorite; (e) grain-supported sandy fine conglomerate(PPL), showing the chlorite coating is developed on the edges of altered tuffaceous fragments; (f) grain-supported medium-fine conglomerate(RL), showing altered tuffaceous fragments and precipitated hematite. Tf: tuffaceous fragments; Ch: chlorite; Ch-C: chlorite coating; Hm: hematite; PPL: plane-polarized light; RL: reflected light.

(1) Tuffaceous fragment alteration

According to Section 4.1.2, the parent rock types of tuffaceous fragments in the Qingshuihe Formation include ultramafic, mafic and intermediate rocks (Fig. 3). The alteration product of ultramafic–mafic tuffaceous fragments in the Gsfc is chlorite (Fig. 9d, e). However, hematite is the alteration product of ultramafic–mafic tuffaceous fragments in the Gmfc (Fig. 9f).

(2) Tuffaceous matrix alteration

Like the tuffaceous fragments, the tuffaceous matrix also underwent apparent alteration. The tuffaceous matrix can transform into chlorite, illite and hematite. First,

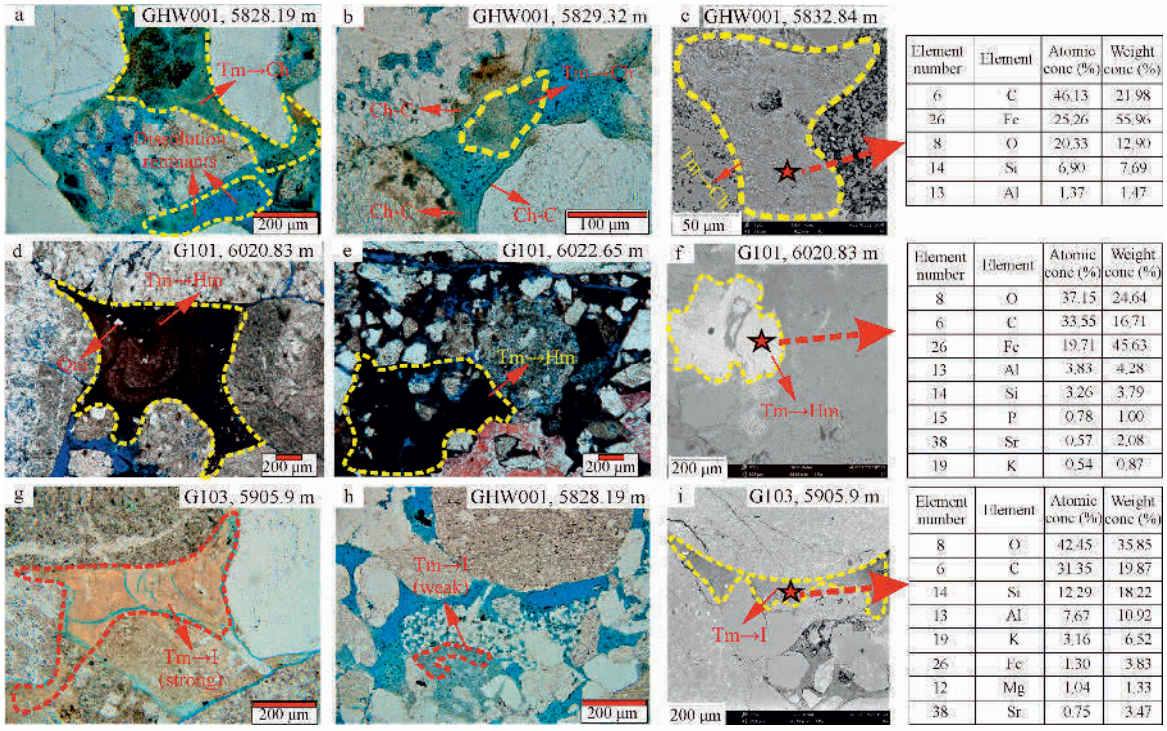

Element number	Element	Atomic conc (%)	Weight conc (%)
6	C	46.13	21.98
26	Fe	25.26	55.96
8	O	20.33	12.90
14	Si	6.90	7.69
13	Al	1.37	1.47

Element number	Element	Atomic conc (%)	Weight conc (%)
8	O	37.15	24.64
6	C	33.55	16.71
26	Fe	19.71	45.63
13	Al	3.83	4.28
14	Si	3.26	3.79
15	P	0.78	1.00
38	Sr	0.57	2.08
19	K	0.54	0.87

Element number	Element	Atomic conc (%)	Weight conc (%)
8	O	42.45	35.85
6	C	31.35	19.87
14	Si	12.29	18.22
13	Al	7.67	10.92
19	K	3.16	6.52
26	Fe	1.30	3.83
12	Mg	1.04	1.33
38	Sr	0.75	3.47

Fig. 10. Characteristics of tuffaceous matrix alteration and its element geochemical response in the Qingshuihe Formation clastic rock reservoirs of Gaoquan area, Sikeshu sag.

(a, b) Tuffaceous matrix transform to chlorite (grain-supported sandy fine conglomerate, PPL); (c) SEM and EDS of marked site showing the Fe-rich tuffaceous matrix; (d, e) tuffaceous matrix transform to hematite, and some microcrystalline quartz can be seen in the matrix (grain-supported medium-fine conglomerate, PPL); (f) SEM and EDS of marked site showing the Fe-rich tuffaceous matrix; (g) tuffaceous matrix transform to illite is very strong (matrix-supported medium conglomerate, PPL); (h) tuffaceous matrix transform to illite is very weak (grain-supported sandy fine conglomerate, PPL); (i) SEM and EDS of marked site showing the K-rich tuffaceous matrix. Tm→Ch: tuffaceous matrix transform into chlorite; Tm→Hm: tuffaceous matrix transform into hematite; Tm→I: tuffaceous matrix transform into illite; Qm: microcrystalline quartz; Ch-C: chlorite coating; PPL: plane-polarized light; CPL: cross-polarized light.

transforming the tuffaceous matrix to chlorite primarily occurred in the Gsfc. In the chloritized tuffaceous matrix, needle-shaped chlorite usually distributes in the matrix or develops on the edge of the detrital particles (Fig. 10a, b). The EDS analysis shows that the chloritized tuffaceous matrix contains abundant Fe elements (Fig. 10c).

In addition to chlorite, the Fe-rich tuffaceous matrix can also be transformed into hematite, primarily occurring in the Mmc or Gmfc. The colour of the hematized tuffaceous matrix is brown or deep brown under plane-polarized light, and the microcrystalline quartz produced by devitrification can be observed in the tuffaceous matrix (Fig. 10d, e). The EDS analysis shows that the hematized tuffaceous matrix is also rich in Fe elements (Fig. 10f).

The tuffaceous matrix can be transformed not only into ferruginous minerals but also into illite. This alteration phenomenon is more evident in Mmc and Gmfc (Fig. 10g) but not in Gsfc (Fig. 10h). The fibrous-shaped illite formed by tuffaceous matrix alteration is light yellow under plane-polarized light (Fig. 10g). SEM and EDS analyses show that the tuffaceous matrix that can transform into illite has high K and low Fe and Mg (Fig. 10i).

4.3.3 Tuffaceous component dissolution

Dissolution is a critical factor in improving the quality of clastic rock reservoirs (Mansurbeg et al., 2008; Morad et al., 2010). Two kinds of dissolution exist in the clastic rock reservoirs of the Qingshuihe Formation, such as tuffaceous fragments and tuffaceous matrix dissolution. The dissolution characteristics of tuffaceous components are significantly different under the backgrounds of different depositional units and lithofacies.

(1) Tuffaceous fragment dissolution

The dissolution intensity of tuffaceous fragments in Mmc and Gmfc is typically weak but strong in Gsfc. For example, the feldspars in tuffaceous fragments have no noticeable dissolution in Mmc and Gmfc but are almost entirely dissolved in Gsfc (Fig. 11a, b).

(2) Tuffaceous matrix dissolution

According to the analysis results in Section 4.3.2, the hematitization and illitization of the tuffaceous matrix in Mmc and Gmfc are common, resulting in only a few tuffaceous matrices dissolved (Fig. 11c, d). However, the Fe- and K-rich tuffaceous matrix in the Gsfc has an apparent dissolution (Fig. 11e, f). Chlorite coating can be observed on the edges of detrital particles around the remnants of the Fe-rich tuffaceous matrix after the dissolution (Figs. 10a, 11e).

4.4 Reservoir quality

The lithofacies and the parent rock types noticeably affect the reservoir physical properties (Liu et al., 2012; Hou et al., 2013; Kra et al., 2022; Yang et al., 2022). From

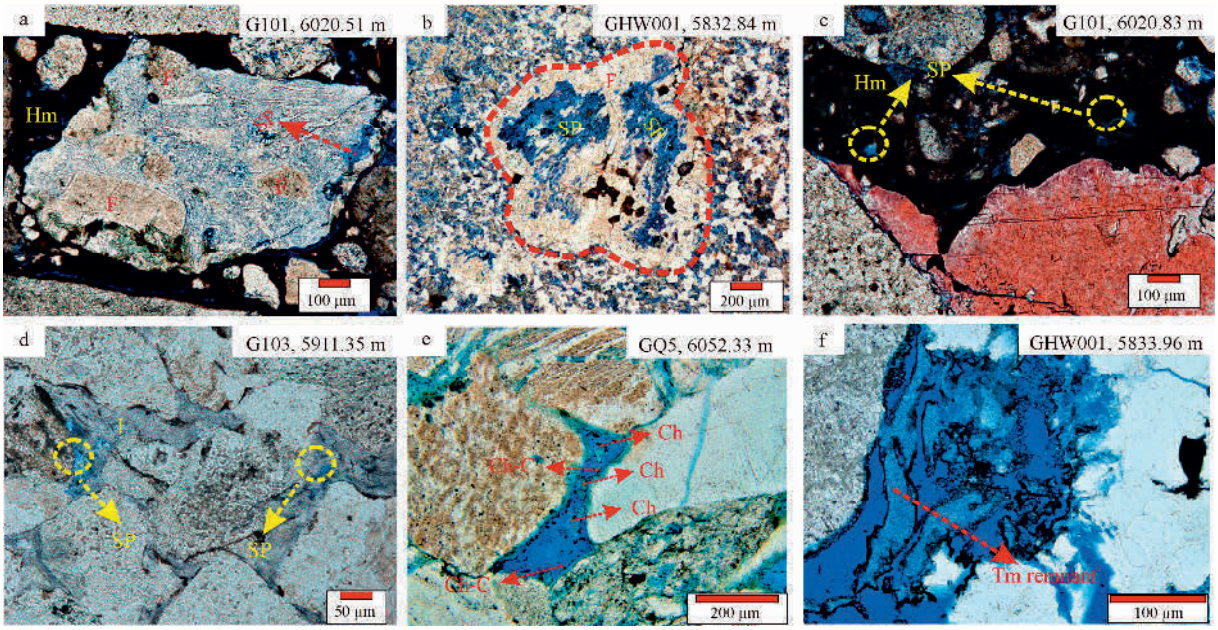

Fig. 11. Dissolution characteristics of tuffaceous fragments and tuffaceous matrix in the Qingshuihe Formation clastic rock reservoirs of Gaoquan area, Sikeshu sag.

(a) Photomicrograph of the thin section showing the feldspathic phenocryst of tuffaceous fragments has a weak dissolution (grain-supported medium–fine conglomerate, PPL); (b) photomicrograph of the thin section showing the feldspars in tuffaceous fragment has a strong dissolution (grain-supported sandy fine conglomerate, PPL); (c) photomicrograph of the thin section showing the tuffaceous matrix transform to hematite and has a weak dissolution (grain-supported medium–fine conglomerate, PPL); (d) photomicrograph of the thin section showing the tuffaceous matrix transform to illite and has a weak dissolution (matrix-supported medium conglomerate, PPL); (e) photomicrograph of the thin section showing the Fe-rich tuffaceous matrix is dissolved and chlorite coating is developed on the edge of clastic particles around the tuffaceous matrix remnant (grain-supported sandy fine conglomerate, PPL); (f) photomicrograph of the thin section showing the K-rich tuffaceous matrix without alteration has a strong dissolution (grain-supported sandy fine conglomerate, PPL). Tf: tuffaceous fragments; Tm: tuffaceous matrix; F: feldspar; Hm: hematite; Ch: chlorite; Ch-C: chlorite coating; I: illite; SP: secondary pore; PPL: plane-polarized light.

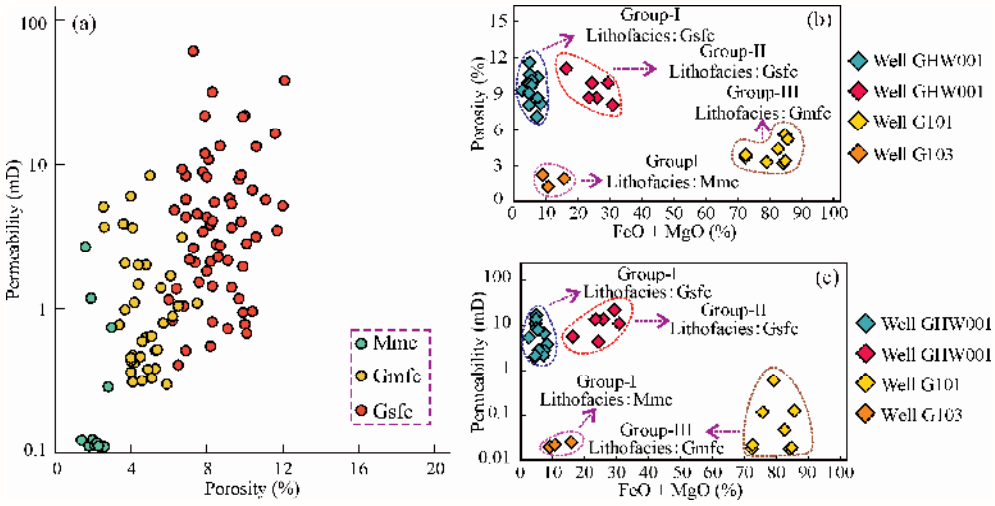

Fig. 12. Characteristics of tuffaceous clastic rock reservoirs properties of Qingshuihe Formation in the Gaoquan area, Sikeshu sag.

(a) Plots of the relationship between porosity and permeability of different lithofacies from the test and collected data; (b) the distribution characteristic of porosity in different tuffaceous matrix; (c) the distribution characteristic of permeability in different tuffaceous matrix. Mmc: matrix-supported medium conglomerate; Gmfc: grain-supported medium-fine conglomerate; Gsfc: grain-supported sandy fine conglomerate.

a lithofacies perspective, the porosity of Gsfc ranges from 6.0% to 17.4% (avg. 8.8%) and the permeability is 0.26–61.70 mD (avg. 7.0 mD) (Fig. 12a). The porosity of Gmfc ranges from 2.6 to 8.2% (avg. 4.9%), and the permeability ranges from 0.29 to 6.06 mD (avg. 1.51 mD) (Fig. 12a). The porosity of Gmfc is 1.0%–3.8% (avg. 2.3%). The permeability is 0.03 to 2.71 mD (avg. 0.46 mD) (Fig. 12a). Overall, the physical properties of Gsfc are good. However, the Mmc and Gmfc are poor.

The proportion of tuffaceous matrix in interstitial

materials is the highest (Fig. 2c), also noticeably influencing the reservoir physical properties. The Qingshuihe Formation has three tuffaceous matrix types (Fig. 5). The porosity of reservoirs containing Group-II ranges from 8.1% to 11.1%, and the permeability from 4.34 to 21.70 mD, which belongs to the high-quality reservoirs (Fig. 12b, c). However, the porosity of reservoirs containing Group-III is 3.2%–5.6%, and the permeability is 0.02–6.92 mD, which belongs to the poor reservoirs (Fig. 12b, c). The parts of the reservoirs containing Group-I are high-quality reservoirs, and their porosity is 7.6%–11.1% and permeability is 1.95–16.00 mD (Fig. 12b, c). However, other parts of reservoirs containing Group-I are poor reservoirs, with porosity less than 3.0% and permeability less than 0.02 mD (Fig. 12b, c).

5 Discussion

5.1 Impact of sedimentation and parent rock on diagenesis

5.1.1 Impact of sedimentation on diagenesis

The original physical property and the pore structure of clastic rocks influence the diagenetic reformation of reservoirs (Morad et al., 2000; Mansurbeg et al., 2008; Dutton and Loucks, 2010; Bjørlykke, 2014). Studies have shown that sedimentation controls the original physical properties of reservoirs (Morad et al., 2000). Different sedimentary systems have different hydrodynamic environments, transport distances of sediments, textural maturity and compositional maturity, resulting in other depositional units developing different lithofacies (Liu et al., 2022; Wu et al., 2022). Due to the various original physical properties and pore structures of different lithofacies, the closure intensity of the corresponding geochemical system has differed before the burial stage, and the subsequent diagenetic intensity differs.

The main channels of the upper fan delta plain and distributary channels of the lower fan delta plain are close to the provenance, the fluid types are dominated by debris flow with high density and viscosity, and the proportion of traction current is low (e.g., wells G103 and G101; Figs. 7, 13; Supp. Table 1). Consequently, Mmc and Gmfc have poor sorting and high matrix content (Supp. Table 1; Figs. 6a, b, 14a, b), resulting in strong compaction condition and closed original geochemical system. The desulfurization and metamorphism coefficients of formation water can indirectly reflect the closure degree of geochemical system (Chen et al., 2012). The metamorphic coefficient and desulfurization coefficient of Mmc and Gmfc are 0.6–0.9 and 0.6–5.0, which indirectly indicate that the geochemical system of Mmc and Gmfc is much closed (Fig. 15). The exchange degree of materials in the reservoir depends on the sealing degree of the geochemical system (Giles and De Boer, 1990; Higgs et

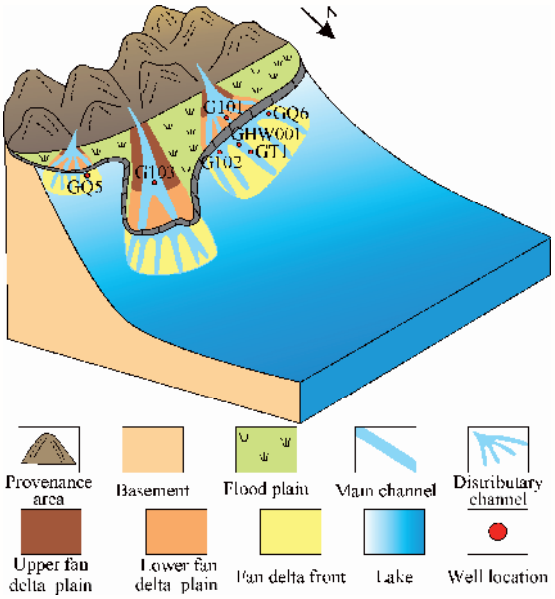

Fig. 13. The sedimentary facies distribution of Qingshuihe Formation in the Gaoquan area, Sikeshu sag.

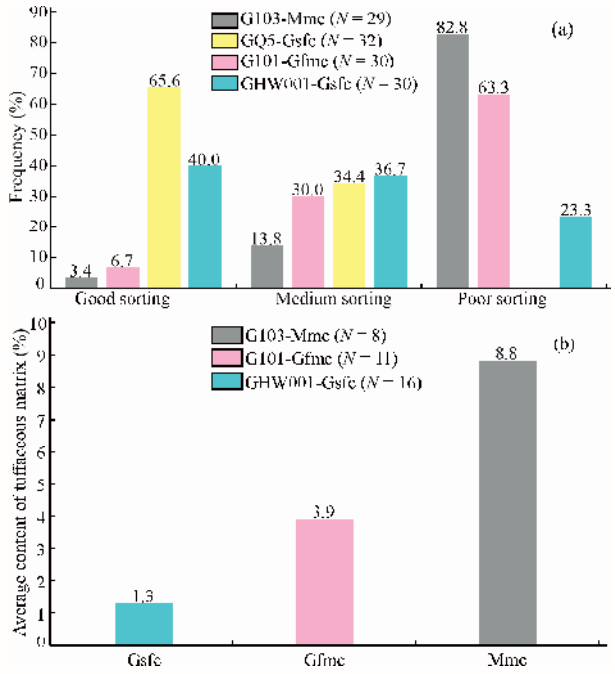

Fig. 14. The characteristics of sorting and matrix content of different lithofacies of Qingshuihe Formation in the Gaoquan area, Sikeshu sag.

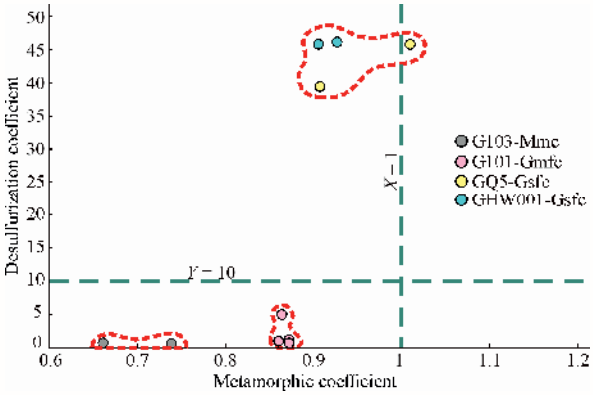

Fig. 15. Desulfurization coefficient and metamorphism coefficient of formation water in different lithofacies of Qingshuihe Formation in Gaoquan area of Sikeshu depression.

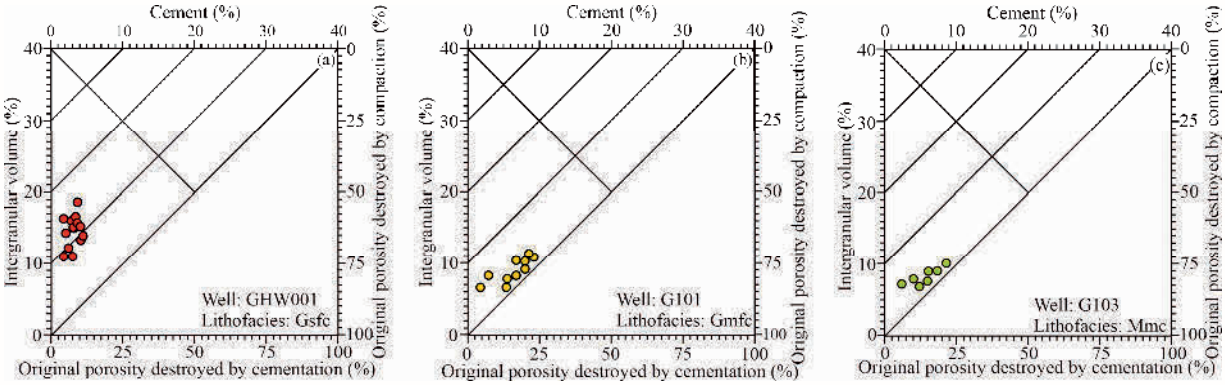

Fig. 16. Plot of intergranular volume (IGV) versus volume of cement in the Qingshuihe Formation tuffaceous clastic reservoirs of different sedimentary facies and lithofacies.
According to the diagram proposed by Houseknecht (1987), assuming an original porosity of 40%. Mmc: matrix-supported medium conglomerate; Gmfc: grain-supported medium-fine conglomerate; Gsfc: grain-supported sandy fine conglomerate.

al., 2007; Molenaar et al., 2015; Yuan et al., 2017). When the geochemical system is very closed, the alkaline ions in the pore fluids are oversaturated and precipitate many diagenetic minerals in the pores (Bjørlykke and Jahren, 2012; Yuan et al., 2015). Therefore, Mmc and Gmfc also have the characteristics of strong cementation and weak dissolution (Figs. 10d, e, g, 11a, b, f, g).

Compared with the fan delta plain, the underwater distributary channels of the fan delta front belong to the traction current category, which has a strong hydrodynamic environment (e.g., wells GQ5 and GHW001; Figs. 7, 13; Supp. Table 1). The sediments in this depositional unit were adequately washed with high-energy water, improving the grain sorting and decreasing the tuffaceous matrix content between detrital particles (Figs. 6e, f, 14a, b). Therefore, the compaction intensity of Gsfc was noticeably weaker than that of Mmc and Gmfc (Fig. 9c), facilitating the preservation of geochemical system openness and mitigating the damage of mechanical compaction on exchange degree of materials. The formation water characteristics show that the metamorphic coefficient of is 0.9–1.1, and the desulfurization coefficient is 39.4–46.1 (Fig. 15), which indicates that the geochemical chemical system of Gsfc is less closed than that of Mmc and Gmfc. Therefore, when the burial depth is similar, the dissolution intensity in the Gsfc is stronger than Mmc and Gmfc (Fig. 11b, e, f), and the cementation strength is weak (Figs. 9c, 10h). Figure 16 shows that the loss of intragranular volume of Gsfc is lower (COPL is 50%–75%) than that of Mmc and Gmfc (COPL > 75%).

5.1.2 Impact of parent rock on diagenesis

In addition to sedimentation, the geochemical properties of the parent rock also noticeably influence the diagenesis of tuffaceous clastic rock reservoirs (Liu et al., 2012; Hou et al., 2013). Studies have shown that tuffaceous components can inherit the geochemical properties of their parent rocks (Anda, 2012; Hong et al., 2019). However, even if tuffaceous components come from the same parent rock type but the sealing degree of the geochemical system differs, their diagenetic evolutionary results will be significantly influenced. According to the analysis in Section 4.1.2, the diagenetic evolutionary results of tuffaceous components of different lithofacies significantly differ.

First, we will discuss the mechanism of different diagenetic evolutionary results of Fe-rich tuffaceous components. The original geochemical system of Mmc and Gmfc is closed, making it challenging for Fe elements released from Fe-rich tuffaceous components to migrate to other parts of the reservoir, resulting in the concentration of Fe^{2+} in pore water reaching oversaturation. Simultaneously, Mmc and Gmfc were primarily in the oxidised sedimentary environment before the burial stage, which can promote Fe^{2+} to Fe^{3+} transformation through oxidation, forming hematite. However, the Fe-rich tuffaceous matrix in the Gsfc primarily transforms into chlorite, and chlorite coating frequently develops on the edge of the detrital particles (Fig. 10a, b). Studies have shown that Fe and Mg elements can combine with precursor clay minerals and transform into chlorite coating in high-energy hydrodynamic and underwater reductive environments (Cao et al., 2018; Zhao et al., 2022). The Gsfc was in the underwater distributary channels, with high-energy hydrodynamic force and coarse grain size, and the bed load became the critical way to transport the sediments. The laws of fluid mechanics control the transportation and deposition of detrital grains and matrices in a medium (Cao et al., 2018). The high-energy hydrodynamic environment decreases the pressure over the particle surface. Simultaneously, the tuffaceous matrix suspended in water does not move relative to the flow, resulting in a higher pressure over the matrix surfaces than the detrital grain surfaces (Cao et al., 2018). This process leads to the motion between the matrix and detrital grains, leading to the matrix covering the grain surface and forming a coating structure. The tuffaceous matrix can be altered into smectite (Klass et al., 1981; Ahn and Peacor, 1985; Burton et al., 1987). Through the above mechanism, the Fe-rich tuffaceous matrix covering the grain surface can be recrystallised in situ and transformed into chlorite crystals (Billault et al., 2003; Sun et al., 2020). Furthermore, the alteration and dissolution of tuffaceous fragments can provide Fe and Mg elements to form

chlorite coating (Figs. 9d, e, 11d, e).

Similarly, alteration dominates the K-rich tuffaceous matrix due to the poor original physical properties of Mmc and Gmfc. The K elements produced by alteration are difficult to migrate, gradually increasing the K^+ concentration in pore water. Then, these K^+ combine with the smectite produced by tuffaceous matrix alteration and transform it into illite (Fig. 10g). Studies have shown that smectite can combine with K elements to form illite at 20–200°C (Boles and Franks, 1979; Sun et al., 2020). This understanding indicates that during the eodiagenetic to the meso-diagenetic stage, in addition to mechanical compaction, the diagenetic event of Mmc and Gmfc is mainly dominated by the illitization of K-rich tuffaceous matrix, whereas other diagenetic events are weak. However, the Gsfc has an excellent original geochemical system, and K^+ released by tuffaceous matrix alteration is challenging to enrich in pore water, inhibiting the phenomenon of illitization (Fig. 10h). Therefore, when the burial depth is similar, the geochemical system of Gsfc is relatively more open than that of the Mmc and Gmfc due to the weak compaction intensity, and the K-rich tuffaceous components can be fully dissolved by felsic fluids (Fig. 10i).

Based on the above analysis, we established four typical diagenetic types of tuffaceous clastic rock reservoirs of the Qingshuihe Formation in the study area. The chloritization (Type-I) and dissolution (Type-II) of tuffaceous components primarily develop in the underwater distributary channels of the fan delta front. However, the hematitization (Type-III) and illitization (Type-IV) of tuffaceous components primarily occur in the main channels of the upper fan delta plain and the distributary channels of the lower fan delta plain (Fig. 17).

5.2 Impact of sedimentation and diagenesis on reservoir quality

Studies have shown that tuffaceous components have adverse effects on clastic reservoir quality. For example, tuffaceous fragments are ductile with poor compaction resistance, unconducive to preserving intergranular pores (Li et al., 2020; Deng et al., 2022; Gao et al., 2023). The tuffaceous matrix occupied the intragranular volume as the interstitial materials and caused the loss of intergranular pores (Cao B F et al., 2020; Wei et al., 2020, 2021). However, according to the analysis in Section 5.1, the diagenetic evolutionary results of tuffaceous components from different parent rocks are entirely different in different depositional units and lithofacies, and their influences on reservoir quality differ significantly.

The tuffaceous matrix in Mmc and Gmfc easily transforms into hematite and illite. These diagenetic minerals are difficult to dissolve by felsic fluids and occupy many intragranular pores (Fig. 11c, d), which could be unconducive to improving reservoir quality. In Figure 12, we can see that no matter whether the Fe content in the tuffaceous matrix is high (Group-I) or low (Group-III), both the porosity and permeability in Mmc and Gmfc of the fan delta plain are poor (Fig. 12b, c). Furthermore, the loss of Fe caused by the transformation from the Fe-rich tuffaceous matrix to hematite in Mmc and Gmfc makes chlorite coating difficult to develop, causing the poor compaction resistance of tuffaceous fragments and intensifying the loss of intragranular pores during the burial stage. This is another crucial factor causing the poor reservoir quality in the Mmc and Gmfc. There is an apparent negative correlation between tuffaceous fragments' content and porosity in the Mmc and Gmfc (Fig. 18a, b).

However, the Gsfc is in the underwater reductive environment with high-energy hydrodynamic force. They have a good sorting and an open original geochemical system so that the diagenetic evolutionary results of different tuffaceous matrices are conducive to forming high-quality reservoirs. For example, both K-rich and Fe-rich tuffaceous matrices can be fully dissolved by felsic fluids in the diagenetic stage and provide many secondary pores (Figs. 10a, 11h, i). Figure 12 shows that no matter whether the Fe content in the tuffaceous matrix is high (Group-II) or low (Group-I), the porosity and permeability of Gsfc of the fan delta front are significantly higher than in Gmfc and Mmc of the fan delta plain (Fig. 12b, c). Furthermore, the Fe-rich tuffaceous matrices in Gsfc can also transformed into chlorite coating and enhance the compaction resistance of detrital particles (Figs. 10b, 11e, h). Figure 18 shows an apparent positive correlation between tuffaceous fragments' content and porosity in the Gsfc.

Based on the above analysis, sedimentary facies and parent rock types are crucial in controlling the diagenetic evolution of tuffaceous components and reservoir quality. Sedimentary facies are a prerequisite for developing high-quality tuffaceous clastic rock reservoirs. The sedimentary facies determine whether the original physical property is good or poor and whether the original geochemical system is open or closed. It guides the tuffaceous components with different parent rock properties to experience various diagenetic evolutions. In this study, the tuffaceous components developed in the underwater distributary channels of the fan delta front (the primary fluid property is traction current) usually have constructive diagenetic evolutionary results, which are conducive to forming high-quality reservoirs. However, the primary fluid property of the main and distributary channels in the fan delta plain is debris flow, and the tuffaceous components usually have destructive diagenetic evolutionary results, which are unsuitable for forming high-quality reservoirs. Therefore, if we want to find high-quality reservoirs in continental petroliferous basins containing volcanic eruption and delta depositional backgrounds, the exploration targets should focus on the depositional units with high-energy hydrodynamic environments, traction current as the primary fluid property and ultramafic and rocks as the primary parent rock types.

6 Conclusions

(1) The primary lithofacies of the Qingshuihe Formation includes matrix-supported medium conglomerate (Mmc) developed in the main channel of upper fan delta plain, grain-supported medium–fine conglomerate (Gmfc) formed in the distributary channel of

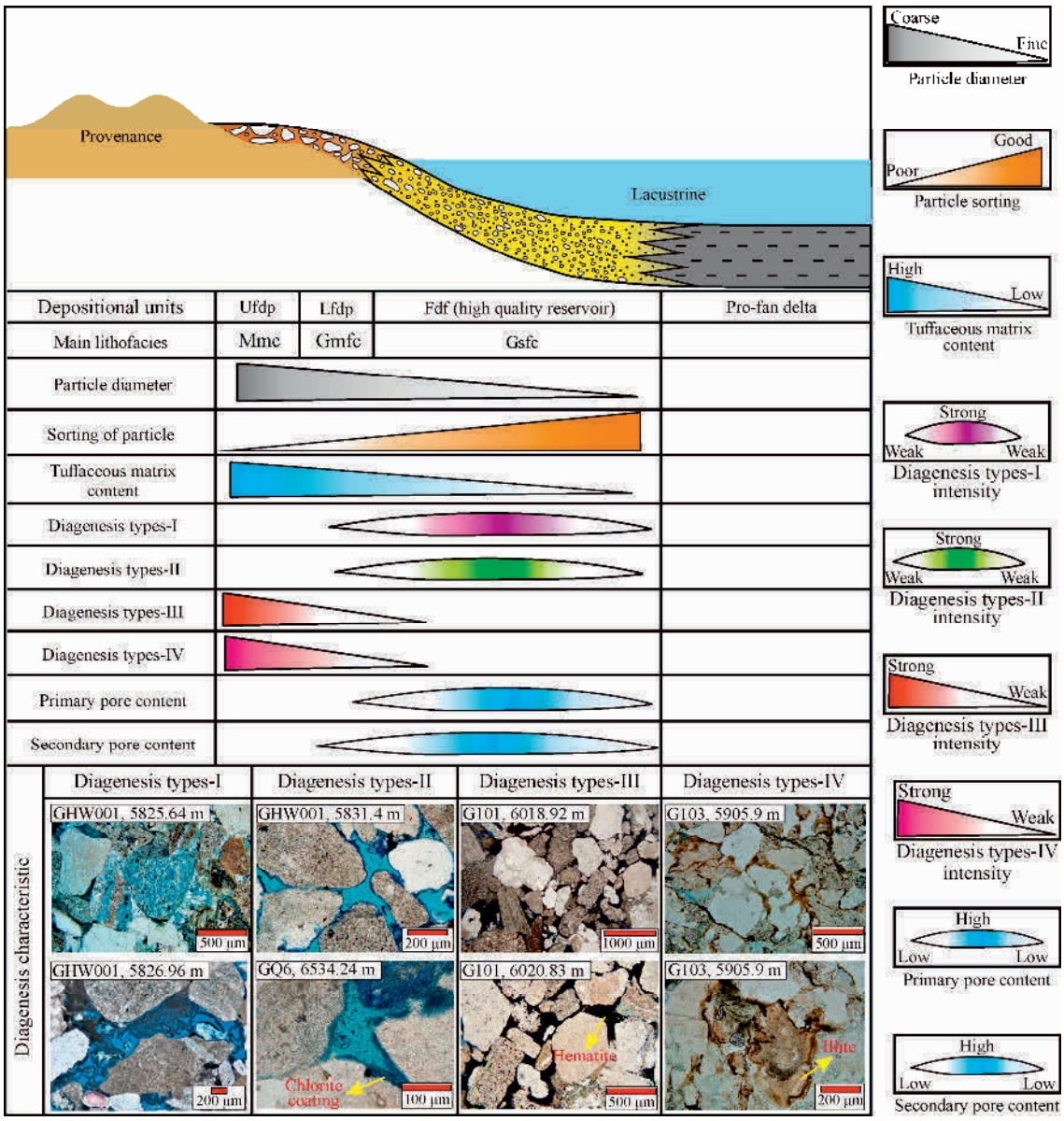

Fig. 17. Diagenesis characteristic of tuffaceous clastic rock reservoirs under different depositional units of Qingshuihe formation, Sikeshu sag.

Ufdp: upper fan delta plain; Lfdp: lower fan delta plain; Fdf: fan delta front; Mmc: matrix-supported medium conglomerate; Gmfc: grain-supported medium-fine conglomerate; Gsfc: grain-supported sandy fine conglomerate; Diagenesis types-I: dissolution; Diagenesis types-II: compaction; Diagenesis types-III: hematite cementation; Diagenesis types-IV: illite cementation.

lower fan delta plain and grain-supported sandy fine conglomerate (Gsfc) developed in the underwater distributary channel of fan delta front.

(2) The skeletal particles and interstitial material in clastic rock reservoirs of the Qingshuihe Formation are dominated by tuffaceous fragments and matrices, respectively. The original parent rock types of tuffaceous fragments and tuffaceous matrices can be classified as ultramafic, mafic and intermediate rocks.

(3) The evolutionary results of tuffaceous components in different lithofacies are significantly different. The tuffaceous components in Mmc and Gmfc mainly transform into hematite and illite, which are difficult to dissolve by felsic fluids. However, the tuffaceous components in Gsfc primarily transform into chlorite coating or are dissolved adequately.

(4) The original geochemical system of Mmc and Gmfc is closed. It has an oxidation environment for a long time, which usually causes the evolutionary results of the tuffaceous components to be unfavourable for preserving primary pores and developing secondary pores. Therefore, the reservoir quality in Mmc and Gmfc is poor.

(5) The original geochemical system of Gsfc is open and in a high-energy hydrodynamic environment, enabling the evolutionary result of the tuffaceous components is usually conducive to the preservation of primary pores and the development of secondary pores. As a result, the reservoir quality of Gsfc is much better than that of the

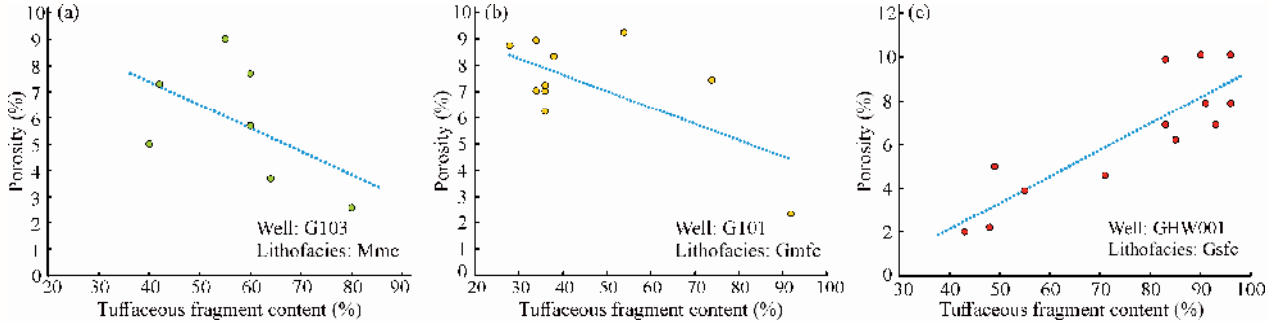

Fig. 18. The relationship between lithofacies, content of tuffaceous fragment and reservoirs porosity of Qingshuihe Formation, Sikeshu sag.
Mmc: matrix-supported medium conglomerate; Gmfc: grain-supported medium-fine conglomerate; Gsfc: grain-supported sandy fine conglomerate.

Mmc and Gmfc, coming the preferred target for oil-gas exploration and development.

(6) The understanding proposed in this study that sedimentary unit, lithofacies and parent rock's geochemical properties jointly control the diagenetic evolution and reservoir quality of tuffaceous clastic rocks provides more guidance for predicting the distribution of high-quality clastic rock reservoirs under the background of volcanic parent rock supply.

Acknowledgments

This work was supported by the National Natural Science Foundation of China (Grant Nos. 42172109, 41872113, 42172108), China National Petroleum Corporation - China University of Petroleum (Beijing) Strategic Cooperation Science and Technology Project (Grant No. ZLZX2020-02), State's Key Project of Research and Development Plan (Grant No. 2018YFA0702405) and Science Foundation of China University of Petroleum (Beijing) (Grant Nos. 2462020BJRC002, 2462020YXZZ020).

Manuscript received Oct. 27, 2023
accepted Dec. 05, 2024
associate EIC: ZHANG Shuichang
edited by GUO Xianqing

Supplementary data to this article can be found online at http: //doi.org/10.1111/1755-6724.15273.

References

Abdel-Fattah, M., Mahdi, A.Q., Theyab, M.A., Pigott, J.D., Abd-Allah, Z.M., and Radwan, A.E., 2022. Lithofacies classification and sequence stratigraphic description as a guide for the prediction and distribution of carbonate reservoir quality: A case study of the Upper Cretaceous Khasib Formation (East Baghdad oilfield, central Iraq). Journal of Petroleum Science and Engineering, 209: 109835.

Ahn, J.H., and Peacor, D.R., 1985. Transmission electron microscopic study of diagenetic chlorite in Gulf Coast argillaceous sediments. Clays and Clay Minerals, 33: 228–236.

Ajdukiewicz, J.M., Nicholson, P.H., and Esch, W.L., 2010. Prediction of deep reservoir quality using early diagenetic process models in the Jurassic Norphlet Formation, Gulf of Mexico. AAPG Bulletin, 94(8): 1189–1227.

Anda, M., 2012. Cation imbalance and heavy metal content of seven Indonesian soils as affected by elemental compositions of parent rocks. Geoderma, 189–190: 388–396.

Antibus, J.V., Panter, K.S., Wilch, T.I., Dunbar, N., McIntosh, W., Tripati, A., Bindeman, I., and Blusztajn, J., 2014. Alteration of volcaniclastic deposits at Minna Bluff: Geochemical insights on mineralizing environment and climate during the Late Miocene in Antarctica. Geochemistry, Geophysics, Geosystems, 15: 3258–3280.

Bajestani, M.S., Mahboubi, A., Moussavi-Harami, R., and Nadjafi, M., 2018. Petrography and geochemistry of sandstones succession of the Qal'eh Dokhtar Formation (Middle-Upper Jurassic), east central Iran: Implications for provenance, tectonic setting and palaeoweathering. Journal of African Earth Sciences, 147: 523–535.

Benavente, C., Mancuso, A., Cabaleri, N., and Gierlowski-Kordesch, E., 2015. Comparison of lacustrine successions and their palaeohydrological implications in two sub-basins of the Triassic Cuyana rift, Argentina. Sedimentology, 62: 1771–1813.

Bien, G.S., Contois, D.E., and Thomas, W.H., 1958. The removal of soluble silica from fresh water entering the sea. Geochimica et Cosmochimica Acta, 14: 35–54.

Billault, V., Beaufort, D., Baronnet, A., and Lacharpagne, J.C., 2003. A nanopetrographic and textural study of grain-coating chlorites in sandstone reservoirs. Clay Minerals, 38: 315–328.

Bjørlykke, K., 2014. Relationships between depositional environments, burial history and rock properties. Some principal aspects of diagenetic process in sedimentary basins. Sedimentary Geology, 301: 1–14.

Bjørlykke, K., and Jahren, J., 2012. Open or closed geochemical systems during diagenesis in sedimentary basins: Constraints on mass transfer during diagenesis and the prediction of porosity in sandstone and carbonate reservoirs. AAPG Bulletin, 96(12): 2193–2214.

Boles, J.R., and Franks, S.G., 1979. Clay diagenesis in Wilcox sandstones of southwest Texas: implications of smectite diagenesis on sandstone cementation. Journal of Sedimentary Research, 49: 55–70.

Burton, J.H., Krinsley, D.H., and Pye, A.K., 1987. Authigenesis of kaolinite and chlorite in Texas Gulf coast sediments. Clays and Clay Minerals, 35: 291–296.

Calvin, C., Diaz, H.G., Mosse, L., Miller, C., and Fisher, K., 2015. Evaluating the Diagenetic Alteration and Structural Integrity of Volcanic Ash Beds within the Eagle Ford Shale. SPE/CSUR Unconventional Resources Conference. Calgary, Alberta, Canada, pp. SPE-175961-MS.

Cao, B.F., Luo, X.R., Zhang, L.K., Lei, Y.H., and Zhou, J.S., 2020. Petrofacies prediction and 3-D geological model in tight gas sandstone reservoirs by integration of well logs and geostatistical modeling. Marine and Petroleum Geology, 114: 104202.

Cao, Y.Y., Chen, F., Zhao, F., Wang, F.J., and Zunu, P., 2020. Tectono-Magmatic events in Junggar Basin during Jurassic period. Xinjiang Geology, 38 (3): 341–347 (in Chinese with English abstract).

Cao, Z., Liu, G.D., Meng, W., Wang, P., and Yang, C.Y., 2018. Origin of different chlorite occurrences and their effects on

tight clastic reservoir porosity. Journal of Petroleum Science and Engineering, 160: 384–392.
Castro, J.M., Beck, P., Tuffen, H., and Nichols, A.R.L., Dingwell, D.B., Martin, M.C., 2008. Timescales of spherulite crystallization in obsidian inferred from water concentration profiles. American Mineralogist, 93: 1816–1822.
Chen, Z.H., Wang S.N., Wang, L., and Zha, M., 2012. Characteristics of formation water chemical fields and its petroleum significance of the Neogene in Dongying Sag，Shandong Province. Journal of Palaeogeography (in Chinese with English abstract), 14(5): 685–693.
Cheng, B., Liu, H., Zhang, K.H., Ren, X.C., Meng, X.Y., Liu, D.Z., 2023. Petroleum in the Jurassic Reservoirs within the Eastern Fukang Sub-depression, Junggar Basin, NW China: Correlation and Source Rock. Acta Geological Sinica (English Edition), 97: 777–795.
Chester, J.S., Lenz, S.C., Chester, F.M., and Lang, R.A., 2004. Mechanisms of compaction of quartz sand at diagenetic conditions. Earth and Planetary Science Letters, 220: 435–451.
Cicerali, D., Arslan, M., Yazar, E.A., Yücel, C., Temizel, İ., Park, S., and Schroeder, P.A., 2020. Mineralogy, chemistry, and genesis of zeolitization in Eocene tuffs from the Bayburt area (NE Turkey): Constraints on alteration processes of acidic pyroclastic deposits. Journal of African Earth Sciences, 162: 103690.
Cui, H., Zhu, S.F., Tan, M.X., and Tong, H., 2022. Depositional and diagenetic processes in volcanic matrix-rich sandstones from the Shanxi and Shihezi formations, Ordos Basin, China: Implication for volcano-sedimentary systems. Basin Research, 34: 1859–1893.
De la Fuente, S., Cuadros, J., Fiore, S., and Linares, J., 2000. Electron microscopy study of volcanic tuff alteration to illite-smectite under hydrothermal conditions. Clays and Clay Minerals, 48: 339–350.
Deng, J.X., Chai, K.W., Song, L.T., Liu, Z.H., Fan, J.G., Tan, K.J., and Wang, B., 2022. The influence of diagenetic evolution on rock physical properties of sandy conglomerate of Baikouquan Formation. Chinese Journal of Geophysics, 65 (11): 4448–4459 (in Chinese with English abstract).
Dickson, J.D., 1965. A modified staining technique for carbonates in thin section. Nature, 205: 587.
Dickson, W.R., Brakenridge, G.R., Erjavec, J.L., Ferguson, R.C., Inman, K.F., Knepp, R.A., Lindberg, F.A., and Ryberg, P,T., 1983. Provenance of North American Phanerozoic sandstones in relation to tectonic setting. GSA Bulletin, 94: 222–235.
Du, J.H., Zhi, D.M., Li, J.Z., Yang, D.S., Tang, Y., Qi, X.F., Xiao, L.X., and Wei, L.Y., 2019. Major breakthrough of Well Gaotan 1 and exploration prospects of lower assemblage in southern margin of Junggar Basin, NW China. Petroleum Exploration and Development, 46(2): 216–227.
Dutton, S.P., and Loucks, R.G., 2010. Diagenetic controls on evolution of porosity and permeability in lower Tertiary Wilcox sandstones from shallow to ultradeep (200–6700 m) burial, Gulf of Mexico Basin, U.S.A. Marine and Petroleum Geology, 27: 59–81.
Ehrenberg, S.N., 1995. Measuring sandstone compaction from modal analyses of thin sections: how to do it and what the results mean. Journal of Sedimentary Research, 65: 369–379.
Fang, X., Yu, X.T., Huang, H.X., Zhang, D.Y., and Zhu, X., 2021. Mineralogical characterization and diagenetic history of Permian marine tuffaceous deposits in Guangyuan area, northern Sichuan basin, China. Marine and Petroleum Geology, 123: 104744.
Fu, Y., Luo, J.L., Shi, X.F., Cao, J.J., Mao, Q.R., and Sheng, W.Y., 2022. Implications of lithofacies and diagenetic evolution for reservoir quality: A case study of the Upper Triassic chang 6 tight sandstone, southeastern Ordos Basin, China. Journal of Petroleum Science and Engineering, 218: 111051.
Gao, C.L., Wang, J., Jin, J., Liu, M., Ren, Y., Liu, K., Wang, K., and Deng, Y., 2023. Heterogeneity and differential hydrocarbon accumulation model of deep reservoirs in foreland thrust belts: A case study of deep Cretaceous Qingshuihe Formation clastic reservoirs in southern Junggar Basin, NW China. Petroleum Exploration and Development, 50(2): 360–372.
Gao, X.Y., Liu, L.F., Jiang, Z.X., Shang, X.Q., and Liu, G.D., 2013. A pre-Paleogene unconformity surface of the Sikeshu Sag, Junggar Basin: Lithological, geophysical and geochemical implications for the transportation of hydrocarbons. Geoscience Frontiers, 4: 779–786.
Garcıá-Romero, E., Vegas, J., Baldonedo, J.L., and Marfil, R., 2005. Clay minerals as alteration products in basaltic volcaniclastic deposits of La Palma (Canary Islands, Spain). Sedimentary Geology, 174: 237–253.
Giles, M.R., and De Boer, R.B., 1990. Origin and significance of redistributional secondary porosity. Marine and Petroleum Geology, 7: 378–397.
Hay, R.L., and Guldman, S.G., 1987. Diagenetic alteration of silicic ash in Searles Lake, California. Clays and Clay Minerals, 35: 449–457.
Hellevang, H., Dypvik, H., Kalleson, E., Pittarello, L., and Koeberl, C., 2013. Can alteration experiments on impact melts from El'gygytgyn and volcanic glasses shed new light on the formation of the Martian surface? Meteoritics & Planetary Science, 48: 1287–1295.
Higgs, K.E., Zwingmann, H., Reyes, A.G., and Funnell, R.H., 2007. Diagenesis, porosity evolution, and petroleum emplacement in tight gas reservoirs, Taranaki Basin, New Zealand. Journal of Sedimentary Research, 77: 1003–1025.
Hong, H.L., Algeo, T.J., Fang, Q., Zhao, L.L., Ji, K.P., Yin, K., Wang, C.W., and Cheng, S., 2019. Facies dependence of the mineralogy and geochemistry of altered volcanic ash beds: An example from Permian-Triassic transition strata in southwestern China. Earth-Science Reviews, 190: 58–88.
Hong, H.L., Fang, Q., Wang, C.W., Churchman, G.J., Zhao, L.L., Gong, N.N., and Yin, K., 2017. Clay mineralogy of altered tephra beds and facies correlation between the Permian -Triassic boundary stratigraphic sets, Guizhou, south China. Applied Clay Science, 143: 10–21.
Hou, L.H., Luo, X., Wang, J.H., Yang, F., Zhao, X., and Mao, Z.G., 2013. Weathered volcanic crust and its petroleum geological significance: A case study of the Carboniferous volcanic crust in northern Xinjiang, NW China. Petroleum Exploration and Development, 40(3): 277–286.
Houseknecht, D.W., 1987. Assessing the relative importance of compaction processes and cementation to reduction of porosity in sandstones. AAPG Bulletin, 71(6): 633–642.
Hu, H.W., Zhang, J., Tian, X.R., Zhuo, Q.G., Jia, C.Z., and Guo, Z.J., 2017. Evolution of the deeply buried Jurassic reservoirs in the southern Junggar Basin, NW China: Evidences from the Well DS-1. Petroleum Research, 2: 247–263.
Irvine, T.H., and Baragar, W.R.A., 1971. A guide to the chemical classification of the common volcanic rocks. Canadian Journal of Earth Sciences, 8: 523–548.
Jin, J., Xian, B.Z., Lian, L.X., Chen, S.R., Wang, J., and Li, J.Q., 2023. Reformation of deep clastic reservoirs with different diagenetic intensities by microfractures during late rapid deep burial: Implications from diagenetic physical simulation of Cretaceous Qingshuihe Formation in the southern margin of Junggar Basin, NW China. Petroleum Exploration and Development, 50(2): 346–359.
Jin, Z.H., Yuan, G.H., Zhang, X.T., Cao, Y.C., Ding. L., Li, X.Y., and Fu, X.H., 2023. Differences of tuffaceous components dissolution and their impact on physical properties in sandstone reservoirs: A case study on Paleogene Wenchang Formation in Huizhou-Lufeng area, Zhu I Depression, Pearl River Mouth Basin, China. Petroleum Exploration and Development, 50(1): 111–124.
Kiipli, T., Kiipli, E., Kallaste, T., Hints, R., Somelar, P., and Kirsimäe, K., 2007. Altered volcanic ash as an indicator of marine environment, reflecting ph and sedimentation rate-example from the Ordovician Kinnekulle bed of Baltoscandia. Clays and Clay Minerals, 55: 177–188.
Klass, M.J., Kersey, D.G., Berg, R.R., and Tieh, T.T., 1981. Diagenesis and secondary porosity in Vicksburg sandstones, McAllen Ranch field, Hidalgo County, Texas. AAPG Bulletin, 65: 1677–1678.
Kra, K.L., Qiu, L.W., Yang, Y.Q., Yang, B.L., Ahmed, K.S.,

Camara, M., and Kouame, E.M., 2022. Depositional and diagenetic control on conglomerate reservoirs: An example from the fourth member of shahejie formation in the Lijin Sag, Bohai Bay Basin, east China. Journal of Petroleum Science and Engineering, 218: 110913.

Lai, J., Bai, T.Y., Li, H.B., Pang, X.J., Bao, M., Wang, G.W., Liu, B.C., and Liu, S.C., 2023. Geological and engineering 'sweet spots' in the Permian Lucaogou Formation, Jimusar Sag, Junggar Basin. Acta Geological Sinica (English Edition), 97: 1214–1228.

Li, G.X., Qin, J.H., Xian, C.G., Fan, X.B., Zhang, J., and Ding, Y., 2020. Theoretical understandings, key technologies and practices of tight conglomerate oilfield efficient development: A case study of the Mahu oilfield, Junggar Basin, NW China. Petroleum Exploration and Development, 47(6): 1275–1290.

Li, Z., Tang, W.X., Peng, S.T., and Xu, J.Q., 2012. Detrital zircon U-Pb geochronological and depositional records of the Mesozoic-Cenozoic profile in the southern Junggar Basin, northwest China, and their responses to basin-range tectonic evolution. Chinese Journal of Geology (Scientia Geologica Sinica), 47(4): 1016–1040 (in Chinese with English abstract).

Liu, G.H., Zhai, G.Y., Huang, Z.L., Zou, C.N., Xia, X.H., Shi, D.S., Zhou, Z., Zhang, C., Chen, R., Yu, S.F., Chen, L., and Zhang, S.H., 2019. The effect of tuffaceous material on characteristics of different lithofacies: A case study on Lucaogou Formation fine-grained sedimentary rocks in Santanghu Basin. Journal of Petroleum Science and Engineering, 179: 355–377.

Liu, H., Jiang, Z.X., Zhang, R.F., and Zhou, H.W., 2012. Gravels in the Daxing conglomerate and their effect on reservoirs in the Oligocene Langgu Depression of the Bohai Bay Basin, North China. Marine and Petroleum Geology, 29: 192–203.

Liu, J.P., Xian, B.Z., Tan, X.F., Zhang, L., Su, M., Wu, Q.R., Wang, Z., Chen, P., He, Y.X., Zhang, S.H., Li, J., Gao, Y., and Yu, Q.H., 2022. Depositional process and dispersal pattern of a faulted margin hyperpycnal system: The Eocene Dongying Depression, Bohai Bay Basin, China. Marine and Petroleum Geology, 135: 105405.

Lundegard, P.D., 1992. Sandstone porosity loss–a "big picture" view of the importance of compaction. Journal of Sedimentary Research, 62: 250–260.

Luo, M., Torres, M.E., Hong, W.L., Pape, T., Fronzek, J., Kutterolf, S., Mountjoy, J.J., Orpin, A., Henkel, S., Huhn, K., Chen, D.C., and Kasten, S., 2020. Impact of iron release by volcanic ash alteration on carbon cycling in sediments of the northern Hikurangi margin. Earth and Planetary Science Letters, 541: 116288.

Mansurbeg, H., Morad, S., Salem, A., Marfil, R., El-ghali, M.A.K., Nystuen, J.P., Caja, M.A., Amorosi, A., Garcia, D., and La Iglesia, A., 2008. Diagenesis and reservoir quality evolution of palaeocene deep-water, marine sandstones, the Shetland-Faroes Basin, British continental shelf. Marine and Petroleum Geology, 25: 514–543.

Martínez-Paco, M., Velasco-Tapia, F., Santana-Salas, L.A., Ju´arez-Arriaga, E., and De Alba, J.A., Ocampo-Díaz, Y.Z.E., 2022. San Felipe and Caracol tuffaceous sandstones, NE Mexico-Late Cretaceous continental arc petrogenetic link: Petrographic, geochemical, and geochronological evidence. Journal of South American Earth Sciences, 116: 103818.

Molenaar, N., Felder, M., Bär, K., and Götz, A.E., 2015. What classic greywacke (litharenite) can reveal about feldspar diagenesis: An example from Permian Rotliegend sandstone in Hessen, Germany. Sedimentary Geology, 326: 79-83.

Morad, S., Al-Ramadan, K., Ketzer, J.M., and De Ros, L.F., 2010. The impact of diagenesis on the heterogeneity of sandstone reservoirs: A review of the role of depositional facies and sequence stratigraphy. AAPG Bulletin, 94(8): 1267–1309.

Morad, S., Ketzer, J.M., and De ros, L.F., 2000. Spatial and temporal distribution of diagenetic alterations in siliciclastic rocks: implications for mass transfer in sedimentary basins. Sedimentology, 47: 95–120.

Rowe, M.C., Ellis, B.S., and Lindeberg, A., 2012. Quantifying crystallization and devitrification of rhyolites by means of X-ray diffraction and electron microprobe analysis. American Mineralogist, 97: 1685-1699.

Rutman, P., Hoareau, G., Kluska, J.M., Lejay, A., Fialips, C., Gelin, F., Aubourg, C., and Bilbao, E.H., 2021. Diagenesis and alteration of subsurface volcanic ash beds of the Vaca Muerta Formation, Argentina. Marine and Petroleum Geology, 132: 105220.

Summa, L.L., and Verosub, K.L., 1992. Trace element mobility during early diagenesis of volcanic ash-Applications to stratigraphic correlation. Quaternary International, 13/14: 149–157.

Sun, N.L., Zhong, J.H., Hao, B., Ge, Y.Z., and Swennen, R., 2020. Sedimentological and diagenetic control on the reservoir quality of deep-lacustrine sedimentary gravity flow sand reservoirs of the Upper Triassic Yanchang Formation in Southern Ordos Basin, China. Marine and Petroleum Geology, 112: 104050.

Tao, Y., Chen, A.Q., Hou, M.C., Niu, C.M., and Wang, Q.B., 2022. Lithofacies characteristics and controlling on volcanic reservoirs in the basement: A case study of the offshore Bohai Bay Basin, Eastern China. Journal of Petroleum Science and Engineering, 209: 109860.

Taylor, T.R., Giles, M.R., Hathon, L.A., Diggs, T.N., Braunsdorf, N.R., Birbiglia, G.V., Kittridge, M.G., Macaulay, C.I., and Espejo, I.S., 2010. Sandstone diagenesis and reservoir quality prediction: Models, myths, and reality. AAPG Bulletin, 94(8): 1093–1132.

Wang, W.R., Yue, D.L., Zhao, J.Y., Li, W., Wang, B., Wu, S.H., and Li, S.H., 2019. Diagenetic alteration and its control on reservoir quality of tight sandstones in lacustrine deep-water gravity-flow deposits: A case study of the Yanchang Formation, southern Ordos Basin, China. Marine and Petroleum Geology, 110: 676–694.

Wei, W., Zhu, X.M., Azmy, K., Zhu, S.F., He, M.W., and Sun, S.Y., 2020. Depositional and compositional controls on diagenesis of the mixed siliciclastic-volcaniclastic sandstones: A case study of the Lower Cretaceous in Erennaoer Sag, Erlian Basin, NE China. Journal of Petroleum Science and Engineering, 188: 106855.

Wei, W., Zhu, X.M., Chen, D.Z., Zhu, S.F., He, M.W., and Sun, S.Y., 2019. Pore fluid and diagenetic evolution of carbonate cements in lacustrine carbonate-siliciclastic rocks: a case from the lower cretaceous of the Erennaoer Sag, Erlian Basin, NE China. Journal of Sedimentary Research, 89: 459–477.

Wei, W., Zhu, X.M., He, M.W., Wang, M.W., and Liu, X.B., 2018. Original sediment composition of the Lower Cretaceous lacustrine tight-oil mudstone and influences on diagenesis and organic matter content, the Erennaoer Sag in Erlian Basin, NE China. Marine and Petroleum Geology, 94: 131–143.

Wei, W., Zhu, X.M., Tan, M.X., Wu C.B.J., Guo, D.B., and Su, H., 2016. Distribution of diagenetic alterations within depositional facies and sequence stratigraphic framework of fan delta and subaqueous fan sandstones: evidence from the Lower Cretaceous Bayingebi Formation, Chagan sag, China–Mongolia frontier area. Geosciences Journal, 20: 1–11.

Wei, W., Zhu, X.M., Zhu, S.F., He, M.W., Sun, S.Y., and Wang, M.W., 2021. Characteristics and control mechanism of high quality reservoir of lacustrine dolomitic rocks from the Lower Cretaceous of the Erennaoer Sag, northeastern China. Earth Science Frontiers, 28(1): 214–224 (in Chinese with English abstract).

Worley, W.G., Tester, J.W., and Grigsby, C.O., 1996. Quartz dissolution kinetics function of pH and from 100–200°C as a ionic strength. AIChE Journal, 42: 3442–3457.

Wu, Q.R., Xian, B.Z., Gao, X.Z., Bai, Q.L., Wang, Z., Liu, J.P., Chen, P., Li, Y.Z., Rahman, N.U., Tian, R.H., Zhang, W.M., and Zhang, H.Z., 2022. Differences of sedimentary triggers and depositional architecture of lacustrine turbidites from normal regression to forced regression: Eocene Dongying depression, Bohai Bay Basin, East China. Sedimentary Geology, 439: 106222.

Xi, K.L., Cao, Y.C., Haile, B.G., Zhu, N., Liu, K.Y., Wu, S.T., and Hellevang, H., 2021. Diagenetic variations with respect to sediment composition and paleo-fluids evolution in conglomerate reservoirs: A case study of the Triassic Baikouquan Formation in Mahu Sag, Junggar Basin,

Northwestern China. Journal of Petroleum Science and Engineering, 197: 107943.
Xi, K.L., Cao, Y.C., Liu, K.Y., Wu, S.T., Yuan, G.H., Zhu, R.K., Kashif, M., Zhao, and Y.W., 2019. Diagenesis of tight sandstone reservoirs in the Upper Triassic Yanchang Formation, southwestern Ordos Basin, China. Marine and Petroleum Geology, 99: 548–562.
Xiao, M., Wu, S.T., Yuan, X.J., Cao, Z.L., and Xie, Z.R., 2020. Diagenesis effects on the conglomerate reservoir quality of the Baikouquan Formation, Junggar Basin, China. Journal of Petroleum Science and Engineering, 195: 107599.
Yang, T., Cao, Y.C., Friis, H., Liu, K.Y., Wang, Y.Z., Zhou, L.L., Yuan, G.H., Xi, K.L., and Zhang, S.M., 2020. Diagenesis and reservoir quality of lacustrine deep-water gravity-flow sandstones in the Eocene Shahejie Formation in the Dongying Sag, Jiyang depression, eastern China. AAPG Bulletin, 104(5): 1045–1073.
Yang, Y.Y., Liu, Y.Q., Šegvić, B., Zhou, D.W., You, J.Y., Jiao, X., Meng, Z.Y., and Zhao, M.R., 2023. Origin, transport, and diagenesis of tuffs in organic-rich lacustrine mudstone: An example from the lower part of the Middle–Late Triassic Chang7 Member, Ordos Basin (NW China). Applied Clay Science, 232: 106790.
Yang, Z., Wu, S.H., Zhang, J.J., Zhang, K., and Xu, Z.H., 2022. Diagenetic controls on the reservoir quality of tight reservoirs in digitate shallow-water lacustrine delta deposits: An example from the Triassic Yanchang Formation, southwestern Ordos Basin, China. Marine and Petroleum Geology, 144: 105839.
Yuan, G.H., Cao, Y.C., Gluyas, J., and Jia, Z.Z., 2017. Reactive transport modeling of coupled feldspar dissolution and secondary mineral precipitation and its implication for diagenetic interaction in sandstones. Geochimica et Cosmochimica Acta, 207: 232–255.
Yuan, G.H., Cao, Y.C., Gluyas, J., Li, X.Y., Xi, K.L., Wang, Y.Z., Jia, Z.Z., Sun, P.P., and Oxtoby, N.H., 2015. Feldspar dissolution, authigenic clays, and quartz cements in open and closed sandstone geochemical systems during diagenesis: Typical examples from two sags in Bohai Bay Basin, East China. AAPG Bulletin, 99(11): 2121–2154.
Zhang, Z.Y., Zhu, G.Y., Chi, L.X., Wang, P.J., Zhou, L., Li, J.F., and Wu, Z.H., 2020. Discovery of the high-yield well GT1 in the deep strata of the southern margin of the Junggar Basin, China: Implications for liquid petroleum potential in deep assemblage. Journal of Petroleum Science and Engineering, 191: 107178.
Zhao, C.J., Jiang, Y.L., Liu, J.D., Liu, M., and Wang, L.J., 2022. Occurrence and origin of chlorite and associated impact on tight sandstone reservoir quality: A case study of the Xujiahe Formation (NE Sichuan Basin, China). Journal of Petroleum Science and Engineering, 209: 109859.
Zheng, H., Sun, X.M., Wang, J.P., Zhu, D.F., and Zhang, X.Q., 2018. Devitrification pores and their contribution to volcanic reservoirs: A case study in the Hailar Basin, NE China. Marine and Petroleum Geology, 98: 718–732.
Zhou, T.Q., Wu, C.D., Yuan, B., Shi, Z.K., Wang, J.L., Zhu,W., Zhou, Y.X., Jiang, X., Zhao, J.Y., Wang, J., and Ma, J., 2019. New insights into multiple provenances evolution of the Jurassic from heavy minerals characteristics in southern Junggar Basin, NW China. Petroleum Exploration and Development, 46(1): 67–81.
Zhou, Y., Liu, Z.L., Mänd, K., Li, F.J., Peng, N., Kuang, H.W., Liu Y.Q., Liu Y.X., and Zhang, M.H., 2022. Geochemical characteristics of Jurassic sandstones on the southern margin of the Junggar Basin: Constraints on provenance and sandstone-type uranium mineralization. Ore Geology Reviews, 146: 104922.
Zhu, S.F., Jia, Y., Cui, H., Dowey, P.J., Taylor, K.G., and Zhu, X.M., 2019. Alteration and burial dolomitization of fine-grained, intermediate volcaniclastic rocks under saline-alkaline conditions: Bayindulan Sag in the Er'Lian Basin, China. Marine and Petroleum Geology, 110: 621–637.
Zhu, S.F., Qin, Y., Liu, X., Wei, C.J., Zhu, X.M., and Zhang, W., 2017. Origin of dolomitic rocks in the lower Permian Fengcheng formation, Junggar Basin, China: evidence from petrology and geochemistry. Mineralogy and Petrology, 111: 267–282.
Zhu, S.F., Zhu, X.M., Jia, Y., Cui, H., and Wang, W.Y., 2020. Diagenetic alteration, pore-throat network, and reservoir quality of tight gas sandstone reservoirs: A case study of the upper Paleozoic sequence in the northern Tianhuan depression in the Ordos Basin, China. AAPG Bulletin, 104(11): 2297–2324.
Zhu, S.F., Zhu, X.M., Liu, X., Wu, D., and Zhao, D.N., 2016. Authigenic minerals and diagenetic evolution in altered volcanic materials and their impacts on hydrocarbon reservoirs: evidence from the lower Permian in the northwestern margin of Junggar Basin, China. Arabian Journal of Geosciences, 9: 97.

About the first author
CHEN Sirui, male, born in 1994 in Langfang, Inner Hebei Province; Ph.D. candidate of China University of Petroleum (Beijing). He is currently interested in the study of formation processes and the distribution laws of oil and gas reservoirs. E-mail: siruichen2020cup@163.com.

About the corresponding author
XIAN Benzhong, male, born in 1973 in Fuling, Inner Chongqing Municipality; Ph.D.; graduated from China University of Petroleum (East China), professor at China University of Petroleum (Beijing). He is currently interested in the study of sedimentation and reservoir geology. E-mail: xianbzh@cup.edu.cn.